| | | | | | |
|---|---|---|---|---|---|
| kawai, H. Hibi, M. Ueda. | Regeneration | s | | | |
| M. Yamagata, A. Yamamoto, E. Kako, N. Kaneko, K. Matsubara, K. Sakai, K. Sawamoto, M. Ueda | Human Dental Pulp-Derived Stem Cells Protect Against Hypoxic-Ischemic Brain Injury in Neonatal Mice | Stroke | Vol.44 No.2 | 551-554 | 2013 |

Research article

# Human dental pulp-derived stem cells promote locomotor recovery after complete transection of the rat spinal cord by multiple neuro-regenerative mechanisms

Kiyoshi Sakai,[1] Akihito Yamamoto,[1] Kohki Matsubara,[1] Shoko Nakamura,[1] Mami Naruse,[1] Mari Yamagata,[1] Kazuma Sakamoto,[2] Ryoji Tauchi,[3] Norimitsu Wakao,[3] Shiro Imagama,[3] Hideharu Hibi,[1] Kenji Kadomatsu,[2] Naoki Ishiguro,[3] and Minoru Ueda[1]

[1]Department of Oral and Maxillofacial Surgery, [2]Department of Biochemistry, and [3]Department of Orthopedic Surgery, Nagoya University Graduate School of Medicine, Nagoya, Japan.

**Spinal cord injury (SCI) often leads to persistent functional deficits due to loss of neurons and glia and to limited axonal regeneration after injury. Here we report that transplantation of human dental pulp stem cells into the completely transected adult rat spinal cord resulted in marked recovery of hind limb locomotor functions. Transplantation of human bone marrow stromal cells or skin-derived fibroblasts led to substantially less recovery of locomotor function. The human dental pulp stem cells exhibited three major neuroregenerative activities. First, they inhibited the SCI-induced apoptosis of neurons, astrocytes, and oligodendrocytes, which improved the preservation of neuronal filaments and myelin sheaths. Second, they promoted the regeneration of transected axons by directly inhibiting multiple axon growth inhibitors, including chondroitin sulfate proteoglycan and myelin-associated glycoprotein, via paracrine mechanisms. Last, they replaced lost cells by differentiating into mature oligodendrocytes under the extreme conditions of SCI. Our data demonstrate that tooth-derived stem cells may provide therapeutic benefits for treating SCI through both cell-autonomous and paracrine neuroregenerative activities.**

## Introduction

The development of effective treatments for spinal cord injury (SCI) has been stifled by this injury's complicated pathophysiology (1). During the acute phase, the focal mechanical insult disrupts tissue homeostasis. This triggers secondary injury processes in which multiple destructive cascades cause the necrotic and apoptotic death of neurons, astrocytes, and oligodendrocytes, which spreads beyond the initial injury site and leads to irreversible axonal damage and demyelination (2, 3). Subsequently, reactive astrocytes and oligodendrocytes near the site of injured spinal cord (SC) respectively produce chondroitin sulfate proteoglycans (CSPGs) and myelin proteins (including myelin-associated glycoprotein [MAG], Nogo, oligodendrocyte myelin glycoprotein [OMgp], netrin, semaphorin, and ephrin). These extracellular molecules function as axon growth inhibitors (AGIs), acting through the intracellular Rho GTPase signaling cascade (4). These multiple pathogenic signals synergistically accelerate the progressive deterioration after SCI. Therefore, therapeutic strategies for functional recovery from SCI must exert multifaceted reparative effects against a variety of pathogeneses (2).

Stem cell–based transplantation therapy holds great promise for establishing such a multifaceted therapeutic strategy. In the last decade, a variety of cell types, including human neural stem cells (5), embryonic stem cell derivatives (6–8), and adult bone marrow stromal cells (BMSCs) (9, 10), have been transplanted into the injured SC of rats or mice, and their neuroregenerative activities evaluated. These preclinical studies showed that engrafted stem cells promote substantial functional recovery after SCI through both cell-autonomous/cell-replacement and paracrine/trophic effects (11). However, the previously tested stem cells show poor survival (6–8, 12) and/or differentiation under the severe conditions of SCI (9, 13, 14), and the transplantation of individual stem cells has led to only modest therapeutic benefits. Furthermore, although the trophic factors derived from these stem cells promote in vitro neurite extension and survival, their roles in the functional recovery of SCI are still largely unknown.

Human adult dental pulp stem cells (DPSCs) and stem cells from human exfoliated deciduous teeth (SHEDs) are self-renewing stem cells residing within the perivascular niche of the dental pulp (15). They are thought to originate from the cranial neural crest and express early markers for both mesenchymal and neuroectodermal stem cells (16, 17). Since naturally exfoliated deciduous and impacted adult wisdom teeth are not usually needed, DPSCs and SHEDs can be obtained without adverse health effects. Similar to BMSCs, these cells are able to differentiate into osteoblasts, chondrocytes, adipocytes, endothelial cells, and functionally active neurons in vitro, under defined conditions (16–19). Trophic factors expressed by them promote neuronal survival, proliferation, differentiation, and migration (20–23). Thus, these previous reports support the use of tooth-derived stem cells as a unique cellular resource for neuroregeneration therapies. However, their ability to promote functional recovery in neurological disorders remains largely unknown.

**Authorship note:** Kiyoshi Sakai and Akihito Yamamoto contributed equally to this work.

**Conflict of interest:** The authors have declared that no conflict of interest exists.

**Citation for this article:** *J Clin Invest.* 2012;122(1):80–90. doi:10.1172/JCI59251.

**Table 1**
Flow cytometry of stem cells from humans

| | SHEDs ($n = 3$) | | DPSCs ($n = 3$) | | BMSCs ($n = 3$) | |
|---|---|---|---|---|---|---|
| | Positive (%) | SD | Positive (%) | SD | Positive (%) | SD |
| **MSC markers** | | | | | | |
| CD90 | 98.25 | 0.91 | 98.96 | 0.95 | ≥90 | |
| CD73 | 91.45 | 8.44 | 96.60 | 2.14 | ≥90 | |
| CD105 | 98.20 | 2.44 | 98.23 | 0.54 | ≥90 | |
| **Negative markers** | | | | | | |
| CD45 | 0.33 | 0.28 | 0.11 | 0.09 | ≤10 | |
| CD34 | 0.36 | 0.32 | 0.07 | 0.03 | ≤10 | |
| CD11b | 0.02 | 0.02 | 0.03 | 0.02 | ≤10 | |
| HLA-DR | 0.45 | 0.39 | 0.12 | 0.10 | ≤10 | |
| **Neural markers** | | | | | | |
| DCX | 95.42 | 0.66 | 84.45 | 0.45 | 91.37 | 8.20 |
| Nestin | 92.71 | 10.46 | 95.40 | 1.52 | 35.76 | 8.06 |
| GFAP | 92.93 | 8.30 | 97.50 | 3.54 | 4.49 | 3.11 |
| βIII-Tubulin | 99.69 | 0.21 | 85.43 | 0.77 | 99.24 | 0.73 |
| NeuN | 31.93 | 7.25 | 26.61 | 4.28 | 2.97 | 1.74 |
| A2B5 | 94.84 | 3.72 | 96.34 | 0.33 | 35.47 | 15.07 |
| CNPase | 99.21 | 0.11 | 98.19 | 0.46 | 21.35 | 7.81 |
| APC | 0.20 | 0.01 | 0.36 | 0.02 | 2.75 | 2.05 |
| MBP | 0.68 | 0.04 | 0.32 | 0.02 | 3.02 | 2.00 |

Here we examined the neuroregenerative activities of DPSCs and SHEDs by transplanting them into a completely transected rat SCI model during the acute phase, in which axonal regeneration rather than axonal sprouting can be evaluated accurately. Our data show that these tooth-derived stem cells promoted functional recovery after SCI by multifaceted neuro-regenerative activities, via both cell-autonomous/cell replacement and paracrine/trophic mechanisms.

## Results

*Characterization of isolated human SHEDs and DPSCs for use in transplantation studies.* Flow cytometry analysis showed that the SHEDs and DPSCs expressed a set of mesenchymal stem cell (MSC) markers (i.e., CD90, CD73, and CD105), but not endothelial/hematopoietic markers (i.e., CD34, CD45, CD11b/c, and HLA-DR) (Table 1). Like human BMSCs, both the SHEDs and DPSCs exhibited adipogenic, chondrogenic, and osteogenic differentiation as described previously (refs. 16, 17, and data not shown). The majority of SHEDs and DPSCs coexpressed several neural lineage markers: nestin (neural stem cells), doublecortin (DCX; neuronal progenitor cells), βIII-tubulin (early neuronal cells), NeuN (mature neurons), GFAP (neural stem cells and astrocytes), S-100 (Schwann cells), and A2B5 and CNPase (oligodendrocyte progenitor cells), but not adenomatous polyposis coli (APC) or myelin basic protein (MBP) (mature oligodendrocytes) (Figure 1A and Table 1). This expression profile was confirmed by immunohistochemical analyses (Figure 1B).

Next, we examined the expression of representative neurotrophic factors by real-time PCR. Both the SHEDs and DPSCs expressed glial cell–derived neurotrophic factor (*GDNF*), brain-derived neurotrophic factor (*BDNF*), and ciliary neurotrophic factor (*CNTF*) at more than 3 to 5 times the levels expressed by skin-derived fibroblasts or BMSCs (Figure 1C).

We further characterized the transcriptomes of SHEDs and BMSCs by cDNA microarray analysis. This gene expression analysis revealed a 2.0-fold difference in the expression of 3,318 of 41,078 genes between SHEDs and BMSCs. Of these, 1,718 genes were expressed at higher levels in the SHEDs and 1,593 genes were expressed at lower levels (data not shown). The top 30 genes showing higher expression in the SHEDs were in the following ontology categories: extracellular and cell surface region, cell proliferation, and tissue/embryonic development (Table 2).

*SHEDs and DPSCs promoted locomotor recovery after SCI.* To compare the neuroregenerative activities of human SHEDs and DPSCs with those of human BMSCs and human skin fibroblasts, we transplanted the cells into the completely transected SCs, as described in Methods, and evaluated locomotion recovery using the Basso, Beattie, Bresnahan locomotor rating scale (BBB scale) (24). Remarkably, the animals that received SHEDs or DPSCs exhibited a significantly higher BBB score during the entire observation period, compared with BMSC-transplanted, fibroblast-transplanted, or PBS-injected control rats (Figure 2A). Importantly, their superior recoveries were evident soon after the operation, during the acute phase of SCI. After the recovery period (5 weeks after the operation), the rats that had received SHEDs were able to move 3 joints of hind limb coordinately and walk without weight support ($P < 0.01$; Supplemental Videos 1 and 2), while the BMSC- or fibroblast-transplanted rats exhibited only subtle movements of 1–2 joints. These results demonstrate that the transplantation of SHEDs or DPSCs during the acute phase of SCI significantly improved the recovery of hind limb locomotor function. Since the level of recovery was similar in the SHED- and DPSC-transplanted rats, we focused on the phenotypical examination of SHED-transplanted rats to elucidate how tooth-derived stem cells promoted the regeneration of the completely transected rat SC.

*SHEDs regenerated the transected corticospinal tract and raphespinal serotonergic axons.* To examine whether engrafted SHEDs affect the preservation of neurofilaments, we performed immunohistochemical analyses with an anti-neurofilament M (NF-M) mAb, 8 weeks after transection. Compared with the PBS-treated control SCs, the SHED-transplanted SCs exhibited greater preservation of NF-positive axons from 3 mm rostral to 3 mm caudal to the transected lesion site (Figure 2, B and C; asterisk indicates epicenter). The percentages of NF-positive axons in the epicenter of the SHED-transplanted and control SCs were 35.8% ± 13.0% and 8.7% ± 3.4%, respectively, relative to sham-treated SCs (Figure 2D).

Regeneration of both the corticospinal tract (CST) and the descending serotonergic raphespinal axons is important for the recovery of hind limb locomotor function in rat SCI. We therefore examined whether these axons had extended beyond the epicenter in the SHED-transplanted SCs. The CST axons were traced with the anterograde tracer biotinylated dextran amine (BDA), which was injected into the sensorimotor cortex. The serotoner-

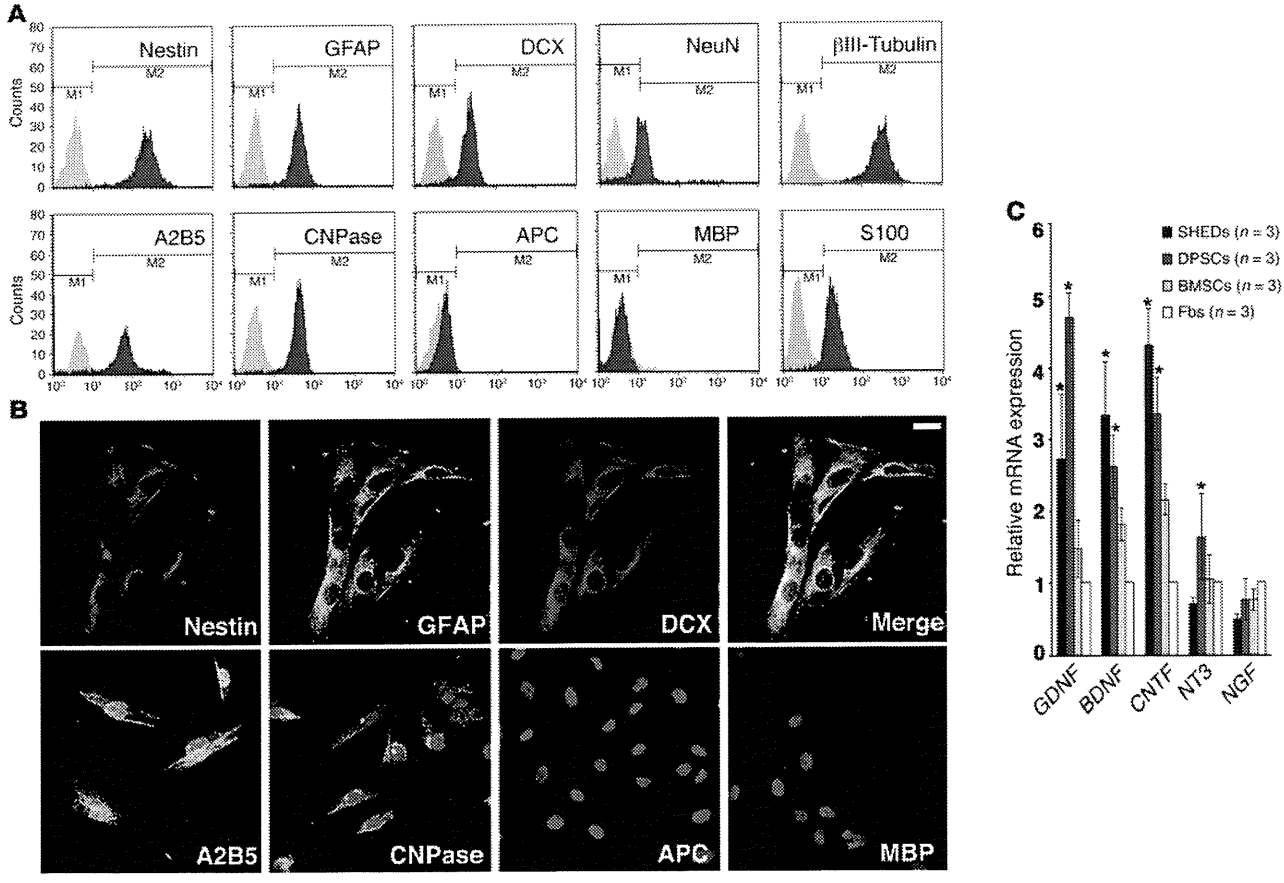


**Figure 1**

Characterization of the SHEDs and DPSCs used for transplantation. (**A**) Flow cytometry analysis of the neural cell lineage markers expressed in SHEDs. Note that most of the SHEDs and DPSCs coexpressed neural stem and multiple progenitor markers, but not mature oligodendrocytes (APC and MBP). (**B**) Confocal images showing SHEDs coexpressed nestin, GFAP, and DCX. SHEDs also expressed markers for oligodendrocyte progenitor cells (A2B5 and CNPase), but not for mature oligodendrocytes (APC and MBP). Scale bar: 10 μm. (**C**) Real-time RT-PCR analysis of the expression of neurotrophic factors. Results are expressed as fold increase compared with the level expressed in skin fibroblasts. Data represent the average measurements for each cell type from 3 independent donors. This set of experiments was repeated twice and yielded similar results. Data represent the mean ± SEM. $^*P < 0.01$ compared with BMSCs and fibroblasts (Fbs).

gic raphespinal axons were immunohistochemically detected by a mAb that specifically reacts with serotonin (5-hydroxytryptamine [5-HT]), which is synthesized within the brain stem. We found that both BDA- and 5-HT–positive fibers extended as far as 3 mm caudal to the epicenter in the SHED-transplanted but not the control group (Figures 3 and 4). Furthermore, some BDA- and 5-HT–positive boutons could be seen apposed to neurons in the caudal stump (Figure 3D and Figure 4C), suggesting that the regenerated axons had established new neural connections. Notably, although the number of descending axons extending beyond the epicenter was small, we observed many of them penetrating the scar tissue of the rostral stump (Figure 3A and Figure 4A). The percentages of 5-HT–positive axons of the SHED-transplanted SCs at 1 and 3 mm rostral to the epicenter were 58.9% ± 3.9% and 78.3% ± 7.4% relative to sham-treated SC, respectively (Figure 4D). These results demonstrate that the engrafted SHEDs promoted the recovery of hind limb locomotion via the preservation and regeneration of transected axons, even in the microenvironment of the damaged CNS.

*SHEDs inhibited the Rho GTPase activity induced by SC transection.* The apparent axon regeneration in the SHED-transplanted SCs suggested that the SHEDs might modulate multiple AGI signals generated from oligodendrocytes and reactive astrocytes forming the glial scar. We therefore measured the activity level of Rho GTPase, which is an intracellular target of multiple AGIs, by pull-down assay. The injured SCs were isolated 7 days after transection and subjected to immunoprecipitation with GST-tagged Rho-binding domain (RBD). The level of active Rho (GTP-bound Rho [GTP-Rho]) in the transected control SCs increased; however, the engrafted SHEDs remarkably inhibited the activation of Rho (Figure 4E). These results strongly suggest that SHEDs promoted axon regeneration through the inhibition of multiple AGI signals.

*Serum-free conditioned medium from both SHEDs and DPSCs antagonizes CSPG- or MAG-mediated neurite growth inhibition.* Next, to analyze the roles of trophic mechanisms in the SHED-mediated axon regeneration, we examined whether the conditioned medium (CM) from SHEDs (SHED-CM) or DPSCs (DPSC-CM) could promote the neurite extension of cerebral granular neurons (CGNs)

**Table 2**
Functional gene classification in SHEDs versus BMSCs

| Term | Changed gene up | Total gene | P |
|---|---|---|---|
| Extracellular region | 343 | 2,865 | $2.52 \times 10^{-14}$ |
| Skeletal system development | 104 | 661 | $1.46 \times 10^{-9}$ |
| Extracellular matrix | 101 | 678 | $9.20 \times 10^{-9}$ |
| Extracellular space | 147 | 1,134 | $2.00 \times 10^{-8}$ |
| Extracellular matrix organization | 43 | 195 | $4.86 \times 10^{-8}$ |
| Multicellular organismal development | 643 | 6,683 | $9.36 \times 10^{-8}$ |
| Collagen fibril organization | 20 | 57 | $4.97 \times 10^{-7}$ |
| Anatomical structure morphogenesis | 346 | 3,339 | $9.52 \times 10^{-7}$ |
| Mitotic cell cycle | 146 | 1,184 | $1.11 \times 10^{-6}$ |
| Proteinaceous extracellular matrix | 82 | 578 | $1.36 \times 10^{-6}$ |
| Organ morphogenesis | 144 | 1,182 | $2.43 \times 10^{-6}$ |
| Vasculature development | 98 | 732 | $3.76 \times 10^{-6}$ |
| Embryonic morphogenesis | 96 | 728 | $7.04 \times 10^{-6}$ |
| Cell proliferation | 245 | 2,288 | $7.17 \times 10^{-6}$ |
| Cell cycle | 230 | 2,135 | $9.74 \times 10^{-6}$ |
| Blood vessel development | 93 | 707 | $1.31 \times 10^{-5}$ |
| Response to wounding | 191 | 1,738 | $2.02 \times 10^{-5}$ |
| Receptor protein serine/ threonine kinase signaling | 56 | 369 | $2.12 \times 10^{-5}$ |
| M phase of mitotic cell cycle | 77 | 567 | $2.40 \times 10^{-5}$ |
| Cell surface | 86 | 671 | $3.26 \times 10^{-5}$ |
| Organ development | 362 | 3,675 | $3.68 \times 10^{-5}$ |
| Collagen binding | 21 | 90 | $3.90 \times 10^{-5}$ |
| Glycosaminoglycan binding | 42 | 262 | $4.65 \times 10^{-5}$ |
| Mitotic spindle organization | 12 | 33 | $7.15 \times 10^{-5}$ |
| Cell adhesion | 183 | 1,693 | $7.76 \times 10^{-5}$ |
| Skeletal system morphogenesis | 42 | 260 | $8.16 \times 10^{-5}$ |
| Tissue development | 185 | 1,720 | $8.76 \times 10^{-5}$ |
| Cell surface receptor linked signaling pathway | 368 | 3,785 | $8.98 \times 10^{-5}$ |
| Mitosis | 73 | 554 | $9.98 \times 10^{-5}$ |
| Regulation of cell cycle | 127 | 1,103 | 0.000109 |

on dishes coated with an AGI. CGNs isolated from newborn rats extended neurites on poly-L-lysine (PLL), but not on CSPG or MAG. Remarkably, both SHED-CM and DPSC-CM restored neurite extension activity of CGNs, while CM from fibroblasts (fibroblast-CM) or BMSCs (BMSC-CM) exhibited only subtle extension (Figure 5). Quantitative analysis showed that neurite extension through the inhibition of multiple AGIs was a unique characteristic of the tooth-derived stem cell (Figure 5, L and M). These results demonstrate that both SHEDs and DPSCs promote the regeneration of transected axons though direct inhibition of the multiple AGI signals by paracrine mechanisms.

*SHEDs inhibited myelin degeneration.* Next, we examined whether transplanted SHEDs preserved myelination in the transected SC by immunohistochemical staining with the fluorescent dye FluoroMyelin. In transverse sections of sham-operated SCs, white matter was clearly labeled by FluoroMyelin, and gray matter was not (data not shown). The control SCs exhibited little or no staining at the epicenter or 3 mm caudal to it (Figure 6, C and D). In contrast, we found significant FluoroMyelin-positive spots in the epicenter of the SHED-transplanted SCs, indicating that the SHEDs caused the regeneration of myelin structures in the transected region (Figure 6A). Notably, the myelin-positive areas of the SHED-transplanted SCs at 3 and 4 mm caudal to the epicenter constituted 55.3% ± 4.5% and 78.0% ± 4.1%, respectively, of the same areas in the sham-operated SCs, demonstrating that the SHEDs exerted remarkable myelin preservation activity (Figure 6E).

*SHEDs survived and specifically differentiated into oligodendrocytes in the injured SC.* In the FluoroMyelin-stained sections, we observed a myelin-expressing cell cluster in the gray matter of SHED-transplanted SCs (Figure 6B). We anticipated that these myelin-expressing cells would be mature oligodendrocytes derived from the transplanted SHEDs. To assess this possibility, we performed immunohistological analyses using anti–human nuclear antigen (HuNu) and two mature oligodendrocyte markers, APC and MBP (25, 26). Eight weeks after grafting, 32.3% ± 3.1% of the transplanted SHEDs still survived in the injured SCs (data not shown). Of these cells, 86.2% ± 6.2% and 90.2% ± 4.6% expressed APC and MBP, respectively (Figure 7). In addition, 10% of the HuNu-positive cells were negative for MBP and APC, but their fate is currently unknown (data not shown). Before the transplantation, SHEDs expressed many early neural cell lineage markers (Figure 1 and Table 1). However, the surviving transplanted SHEDs did not express NF-M or GFAP (Figure 7), indicating that they specifically differentiated along the oligodendrocyte lineage in the injured SCs.

*SHEDs inhibited neuronal and glial apoptosis after SCI.* SCI-induced cell death is a major contributor to secondary injury, in which irreversible tissue damage spreads across the SC. Twenty-four hours after injury, at 1 mm caudal to the epicenter, most of the cells expressing NeuN, GFAP, or MBP were costained with TUNEL, showing that massive multicellular apoptosis occurred immediately after SCI (Figure 8). The engrafted SHEDs significantly decreased the TUNEL staining in all 3 of these lineages (Figure 8, C, D, G, H, K, and L): The total number of TUNEL-positive cells in the SHED-transplanted SCs was approximately 20% of that in the control SCs (Figure 8M). The percentages of TUNEL-positive cells in the control and SHED-transplanted SCs were 87.7% ± 3.1% and 3.1% ± 3.2%, respectively (Figure 8N). These results demonstrate that the transplanted SHEDs minimized the expansion of secondary injury through strong neuroprotection of all the neural cell lineages.

## Discussion

We report here the remarkable neuroregenerative activity of tooth-derived stem cells, SHEDs and DPSCs, for functional recovery after SCI. Previous studies have dealt with the differentiation characteristics of tooth-derived stem cells (16–19) and their trophic effects on the proliferation, migration, and survival of particular subsets of neurons (20–23). However, few studies have considered the therapeutic benefits of these stem cells for a particular neurological disorder. Our study revealed that engrafted SHEDs exhibited three major therapeutic benefits for recovery after SCI, including (a) inhibition of SCI-induced apoptosis of neurons, astrocytes, and oligodendrocytes, which promoted the preservation of neural fibers and myelin sheaths; (b) regeneration of the transected axon through the direct inhibition of multiple AGI signals, such as CSPGs and MAG,

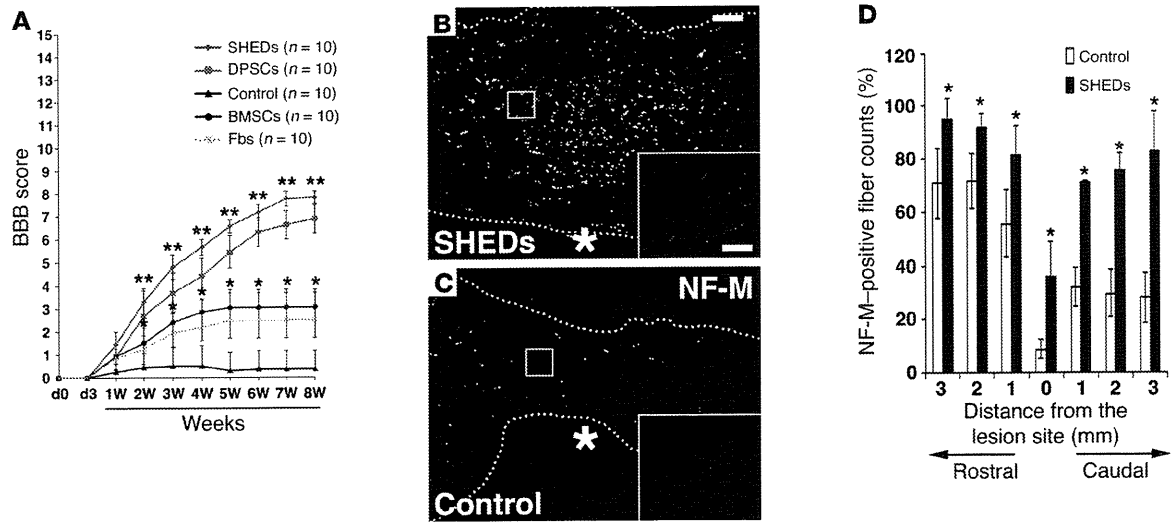


**Figure 2**

Engrafted SHEDs promote functional recovery of the completely transected SC. (**A**) Time course of functional recovery of hind limbs after complete transection of the SC. A total of 1 × $10^6$ SHEDs, DPSCs, BMSCs, or fibroblasts were transplanted into the SCI immediately after transection. Data represent the mean ± SEM. $^{**}P < 0.001$, $^{*}P < 0.01$ compared with SCI models injected with PBS. (**B–D**) Representative images (**B** and **C**) and quantification (**D**) of NF-M–positive nerve fibers in sagittal sections of a completely transected SC, at 8 weeks after SCI. Dashed lines outline the SC. Insets are magnified images of boxed areas in **B** and **C**. (**D**) Nerve fiber quantification, representing the average of 3 experiments performed under the same conditions. The *x* axis indicates specific locations along the rostrocaudal axis of the SC (3 mm rostral and caudal to the epicenter), and *y* axis indicates the percentage of NF-M–positive fibers compared with that of the sham-operated SCs at the ninth thoracic spinal vertebrate (Th9) level. Data represent the mean ± SEM. $^{*}P < 0.05$ compared with SCI models injected with PBS. Scale bars: 100 μm and inset 20 μm (**B**) and 50 μm (**C**). Asterisks in **B** and **C** indicate the epicenter of the lesion.

by paracrine mechanisms; and (c) replacement of lost or damaged oligodendrocytes after SCI through specific differentiation into mature oligodendrocytes under the extreme conditions of SCI. To our knowledge, the latter two neuroregenerative activities (b and c) are unique to tooth-derived stem cells and are not exhibited by any other previously described stem cells. Thus, our data demonstrate that tooth-derived stem cells may provide significant therapeutic benefits for treating the acute phase of SCI through both cell-autonomous and paracrine/trophic regenerative activities.

Adult MSCs have been isolated from various tissues, including bone marrow, adipose tissue, skin, umbilical cord, and placenta (27–30). The therapeutic benefits of these stem cells have drawn intense attention in the field of translational medicine. Nevertheless, their biological equivalency/heterogeneity and identity are largely unknown (31). Tooth-derived stem cells exhibited BMSC-like multipotency and cell surface marker expression; however, they expressed a distinct set of multiple early neural linage markers (Table 1 and Figure 1). A cDNA microarray gene expression analysis showed that the SHEDs expressed many genes in the categories of extracellular and cell surface region, cell proliferation, and tissue/embryonic development, at levels at least 2-fold higher than BMSCs (Table 2). These data indicate that tooth-derived stem cells belong to a highly proliferative ectomesenchymal stem cell–like population that actively communicates with neighboring cells. These characteristics raise the question of what the role of these stem cells is in tooth development and maintenance. Although we do not have a clear answer at present, future analyses using model animals such as dogs and pigs may clarify their precise origin and normal functions, as well as identifying the physiological system that maintains the "stemness" of these cells in vivo.

Both axon regeneration and the reformation of appropriate neuronal connections are prerequisites for functional recovery from SCI. However, multiple AGIs block the inherent regenerative activities of injured axons (2–4). It is well known that multiple AGIs constitute a remarkably intricate molecular network in the extracellular space of the injured CNS, in which they activate a common intracellular signaling mediator, Rho GTPase, and its effector, Rho-associated kinase (ROCK) (32–36). The activation of the Rho-ROCK cascade induces growth cone collapse and axonal repulsion (37). The inactivation of Rho by C3 transferase or of ROCK by Y-27632 downregulates AGI signaling and promotes functional recovery after SCI (38–40). Thus, Rho/ROCK signaling is an important target for SCI treatments; however, no reports have yet described an effect of stem cell transplantation on regulating the multiple AGIs/Rho/ROCK signaling cascades. We found that engrafted SHEDs promoted the regeneration of two major types of descending axons (CST and 5-HT) beyond the lesion epicenter and concomitantly inhibited the SCI-induced Rho activation (Figure 4). Furthermore, both SHED-CM and DPSC-CM promoted the neurite extension of CGNs cultured on two different AGIs, CSPG and MAG (Figure 5). Taken together, these results strongly suggest that tooth-derived stem cells promote the regeneration of transected axons through the direct inhibition of multiple AGI signals by paracrine mechanisms. Notably, in contrast to the CMs from tooth-derived stem cells, BMSC-CM showed only a subtle anti-AGI activity in the neurite extension assay, in good agreement with the level of functional recovery observed in BMSC-transplanted rats. Thus, the anti-AGI activity of tooth-derived stem cells is one of their major therapeutic benefits for the treatment of SCI.

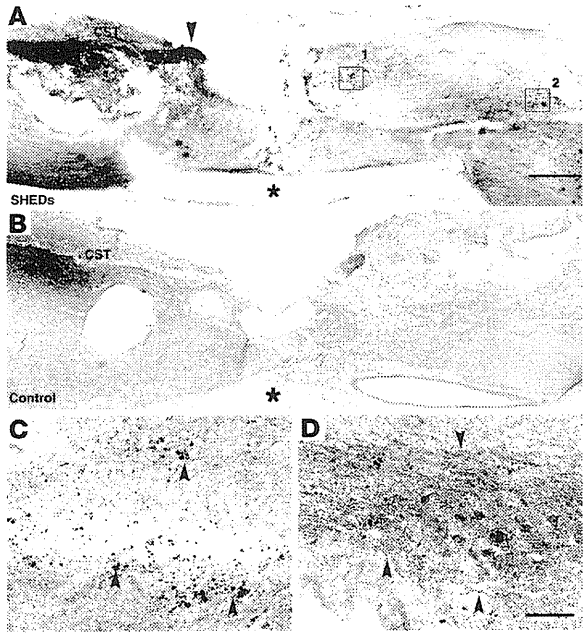


**Figure 3**
SHEDs regenerate CST fibers. Representative images of BDA-labeled CST axons. BDA-positive axons extended beyond the epicenter in the SHED-transplanted (**A**), but not the control SC (**B**). **C** and **D** are high-magnification views of boxed areas 1 and 2 in **A**, respectively. BDA-positive boutons were detected on the neurons of the caudal stump. Scale bars: 500 (**A**) and 100 μm (**D**). Arrowhead in **A** indicates abundant penetration of CST axons into the scar tissue of the rostral stump. Arrowheads in **C** and **D** indicate regenerated CST axons extended beyond the epicenter. Asterisks in **A** and **B** indicate the epicenter of the lesion.

The mechanisms that underlie the inhibition of multiple AGIs by SHED-CM and DPSC-CM are currently unknown. Although both SHEDs and DPSCs expressed an array of neurotrophic factors (Figure 1), our preliminary analysis showed that these trophic factors alone failed to promote the neurite extension of CGNs cultured on CSPG-coated dishes (K. Sakai and A. Yamamoto, unpublished observations). These results suggest that unknown factors, rather than neurotrophic factors, expressed by SHEDs and/or DPSCs may play major roles in the inhibition of multiple AGI signaling pathways. Since the strong anti-AGI activity was unique to the tooth-derived stem cells, but not to BMSCs, extracellular-related genes being preferentially expressed in SHEDs relative to BMSCs (Table 2) is a possible candidate anti-AGI factor. Future functional analysis of these genes will be required to reveal the molecular mechanisms by which tooth-derived stem cells regulate multiple AGI activities to promote the regeneration of injured axons.

It has been shown that pharmacological blockade of neuron and/or oligodendrocyte apoptosis by erythropoietin (41, 42), inhibitors of purine receptor P2X7 (OxATP and PPADS) (43), a neutralizing Ab against CD95 (FAS) antigen (44), or minocycline (45, 46) promotes functional recovery after SCI. We found that engrafted SHEDs suppressed the apoptosis of both neurons and oligodendrocytes (Figure 8), which resulted in the remarkable preservation of neurofilaments and myelin sheaths in the region surrounding the epicenter (Figures 2 and 6). Notably, in addition to these two cell lineages, SHEDs strongly inhibited the apoptosis of astrocytes recruited to the lesion. In the classical view, reactive, CSPG-generating astrocytes are considered to be an obstacle to axon regeneration; however, recent genetic studies in mice have shown that the conditional ablation of astrocytes after SCI resulted in larger lesions, failure of blood brain barrier repair, expansion of the inflammatory response and tissue disruption, severe demyelination, and profound cell death of neurons and oligodendrocytes (47–51). Thus, the accumulated evidence demonstrates that, in addition to their anti-regenerative activity, astrocytes play an important role in the neuroprotection during the acute phase of SCI. We found that SHEDs suppressed the apoptosis of astrocytes and minimized secondary injury but inhibited AGI activity of CSPG derived from activated astrocytes. Thus, these results demonstrate that SHEDs promote the neuroprotective role but inhibit the anti-neuroregenerative activity of astrocytes to promote functional recovery after SCI.

**Figure 4**
SHEDs regenerate 5-HT fibers and inhibit SCI-induced activation of Rho GTPase. (**A–D**) Representative images (**A–C**) and quantification (**D**) of serotonergic raphe axons stained with 5-HT mAb in the sagittal sections of the transected SC. A large number of 5-HT axons penetrated the scar tissue of the rostral stump in the SHED-transplanted SC (**A**), while only a few did in the control transected SC (**B**). (**C**) 5-HT–positive boutons were in contact with neurons of the caudal stump. Arrowhead indicates 5-HT–positive fiber extended beyond the epicenter. Quantification of regenerated 5-HT axons (**D**) was carried out as described in Figure 2D, except the *y* axis indicates the percentage of 5-HT axons compared with that in the sham-operated SC. Data represent the mean ± SEM. $^*P < 0.01$ compared with SCI models injected with PBS. Scale bars: 50 μm (**B** and **C**). (**E**) SCI-induced Rho GTPase activation 7 days after SCI was suppressed by engrafted SHEDs. The level of active Rho in lysate from the samples indicated at the top (sham-operated, control, and SHED-transplanted) was examined by RBD pull-down assay.

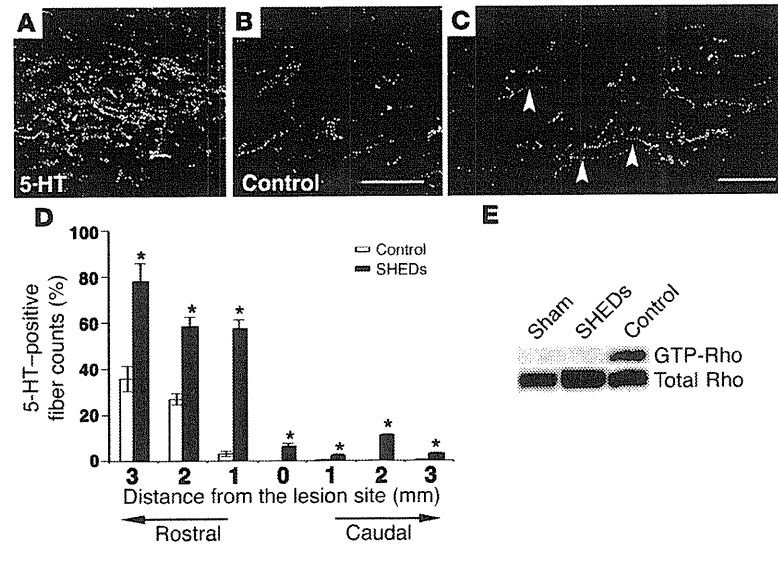

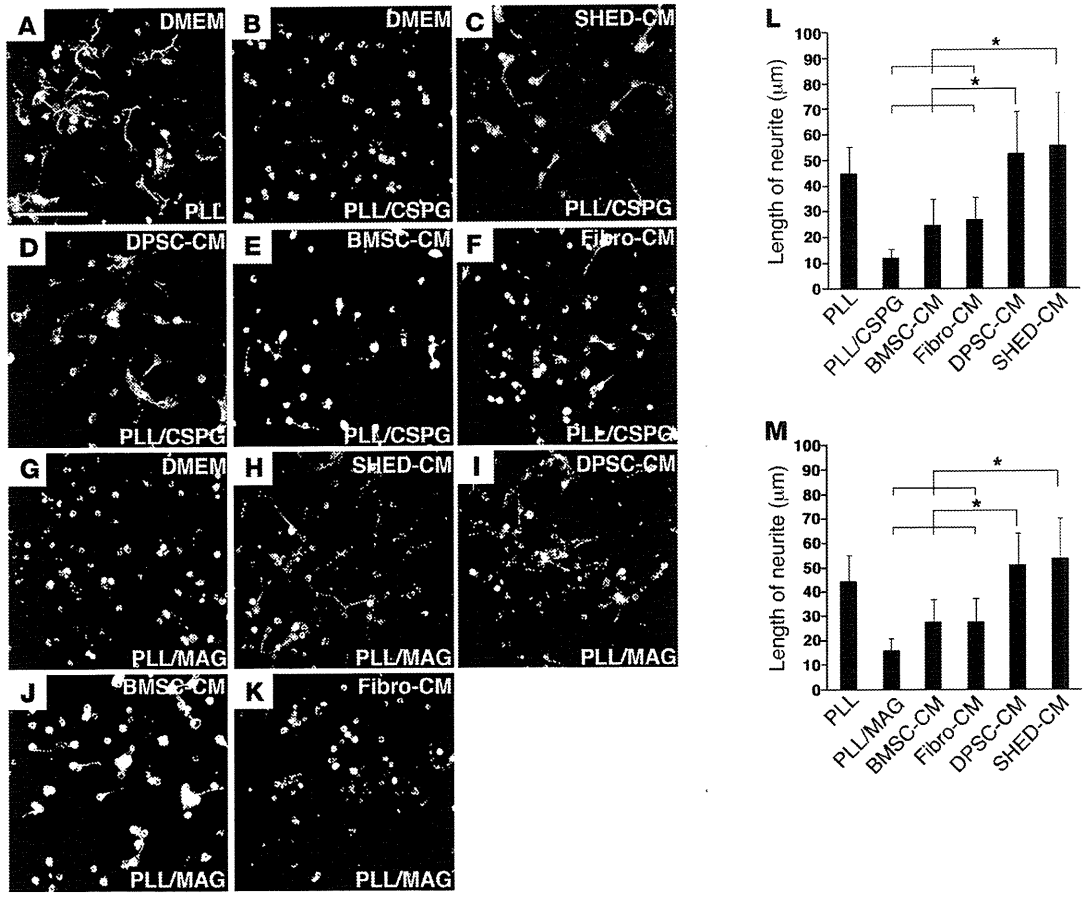


**Figure 5**

SHED-CM and DPSC-CM promote the neurite extension of CGNs on CSPG or MAG. CGNs were plated on PLL (**A**), PLL /CSPG (**B–F**), or PLL /MAG (**G–K**), with the CM indicated at the top of each panel. CGNs plated with SHED-CM or DPSC-CM extended their neurites on the CSPG- (**C** and **D**) and MAG-coated (**H** and **I**) dishes, while BMSC-CM and fibroblast-CM (Fibro-CM) elicited only marginal extension on CSPG (**E** and **F**) and MAG (**J** and **K**). Quantification of the neurite length of CGNs plated on CSPG (**L**) and MAG (**M**). The *y* axis indicates the neurite length. Data represent the average measurements for each cell type from 3 independent donors. This set of experiments was performed 3 times and yielded similar results. Error bars represent SD. $^*P < 0.05$. Scale bar in **A** is 100 μm.

Our data revealed two major advantages of using SHEDs for cell replacement in SCI treatment. First, we observed good survival of the engrafted SHEDs: more than 30% of the engrafted SHEDs survived as a cell mass in the injured SC. A previous study reported that, although the experimental details differed from ours, the survival rate of human ES cell–derived oligodendrocytes or motor neurons, transplanted just after complete SC transection, is less than 1% (8). We speculate that the SHED-mediated minimization of secondary injury and/or the formation of cohesive cell clusters of engrafted SHEDs may be attributable to their excellent cell survival rate. Second, we observed that the engrafted SHEDs specifically differentiated toward mature oligodendrocytes, expressing APC and MBP. It has been shown that DPSCs and SHEDs differentiate in vitro toward functionally active neurons that express voltage-gated $Na^+$ channels and in vivo toward neuron-like cells 48 hours after their transplantation into the mesencephalon of avian embryos (18). Taken together with our findings, these results support the idea that tooth-derived stem cells exhibit neural stem cell–like characteristics and that unknown environmental cues are important for their fate determination. Since cell-based remyelination strategies can restore saltatory conduction and promote functional recovery after SCI (52), the SHED's strong cell survival and oligodendrocyte-specific differentiation potential, particularly under the extreme conditions of SCI, would be great advantages in using these cells to treat SCI. It is hoped that in the future, clarification of the regulatory cues for the specific differentiation of SHEDs will help us to establish efficient therapeutic protocols for SCI patients based on precise cell fate control.

The aim of this study was to address the neuroregenerative activity of tooth-derived stem cells in a particular CNS injury model, SCI. We used the rat complete transection model, because it provides good reproducibility and permits a more accurate assessment of the effects of treatment than do other SCI models. Although contusion and crush models would provide experimental conditions that are closer to the SCIs seen clinically in humans, the amount of injury in these models is not consistent from animal to animal. Furthermore, these incomplete transection models permit spontaneous recovery after SCI, and the residual SC tissues may provide routes for the compensatory sprouting of uninjured SC axons (53). Thus, the transection model was cho-

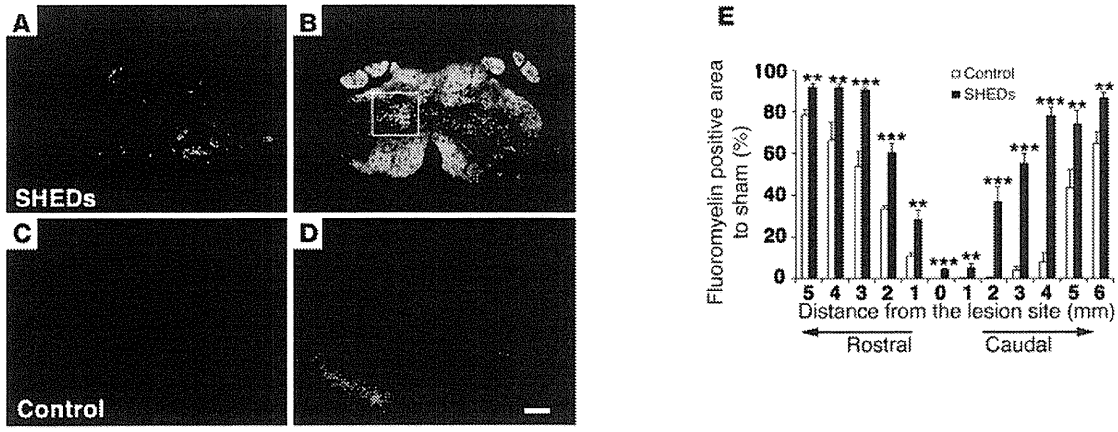


**Figure 6**
SHEDs preserve myelin sheath and differentiate into mature oligodendrocytes in the transected SC. Representative images (**A**–**D**) and quantification (**E**) of the myelinated area 8 weeks after SCI. Transverse sections of the epicenter (**A** and **C**) and 3 mm caudal to it (**B** and **D**) were stained with FluoroMyelin. The myelinated area in both regions was significantly preserved in the SHED-transplanted SC (**A** and **B**), but abolished in the control SC (**C** and **D**). Scale bar: 100 μm (**D**). (**E**) Quantification of the myelinated area showing the average of 3 experiments performed in parallel. The *x* axis indicates specific locations along the rostrocaudal axis of the SC. The *y* axis indicates the percentage of the myelin-positive area compared with that of the sham-operated SC at the Th9 level. Error bars represent SD. $^{**}P < 0.01$, $^{***}P < 0.001$ compared with SCI models injected with PBS.

sen as most appropriate for the precise assessment of the axonal regeneration activity of tooth-derived stem cells.

In this study, we transplanted cells into the injured SC immediately after surgical transection, which is impractical for most human SCI cases. We chose this system to examine the therapeutic benefits of the transplanted cells in countering the multiple pathogenic signals that function synergistically during the early phase of SCI. Our future studies will analyze the neuroregenerative activities of tooth-derived stem cells in SCI under more clinically relevant experimental conditions.

In conclusion, we demonstrated multifaceted neuroregenerative activities of tooth-derived stem cells that fulfill many requirements for functional recovery after SCI. Not only did engrafted SHEDs have remarkable neuroregenerative activities, they also showed no malignant transformation 8 weeks after implantation (data not shown). Furthermore, SHEDs and DPSCs can be obtained from exfoliated deciduous and impacted adult wisdom teeth without adverse health effects. Thus, there are few ethical concerns regarding their clinical use. We propose that tooth-derived stem cells may be an excellent and practical cellular resource for the treatment of SCI.

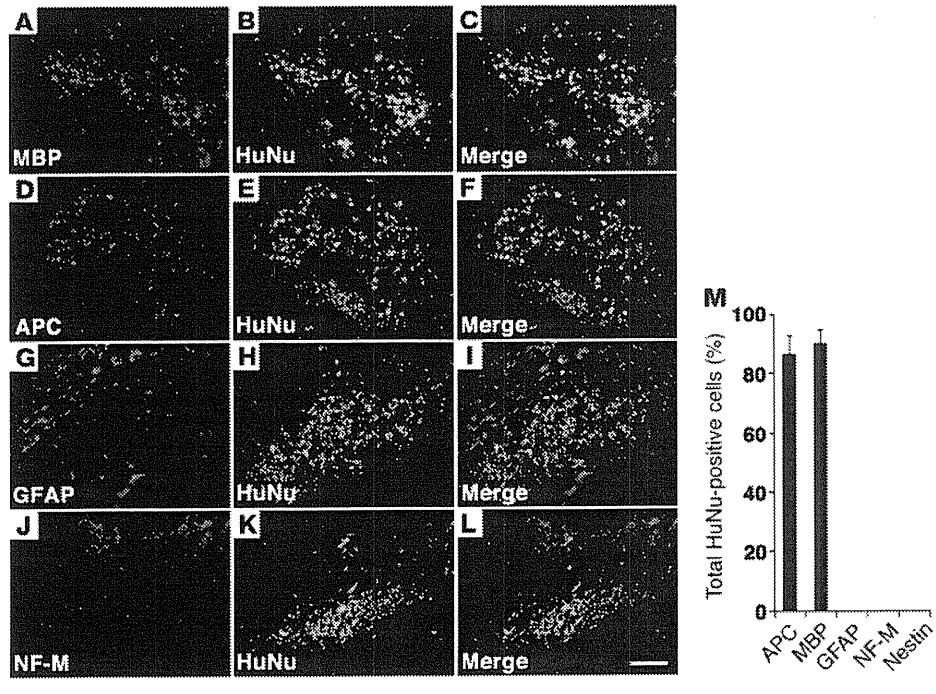


**Figure 7**
SHEDs differentiate into mature oligodendrocytes in the transected SC. A myelin-positive cell cluster ectopically identified in the medulla of a SHED-transplanted SC (boxed area in Figure 6B) was characterized by immunohistochemical staining with an anti–human nuclei mAb (HuNu) together with Abs against neural cell lineage markers: anti-MBP (**A**–**C**), anti-APC (**D**–**F**), anti-GFAP (**G**–**I**), or anti–NF-M (**J**–**L**). The data indicate that SHEDs specifically differentiate into mature oligodendrocytes. The percentage of the lineage marker–positive to total HuNu-positive cell number (**M**) represents the average of 3 experiments performed in parallel. Error bars represent SD. Scale bar: 100 μm (**L**).

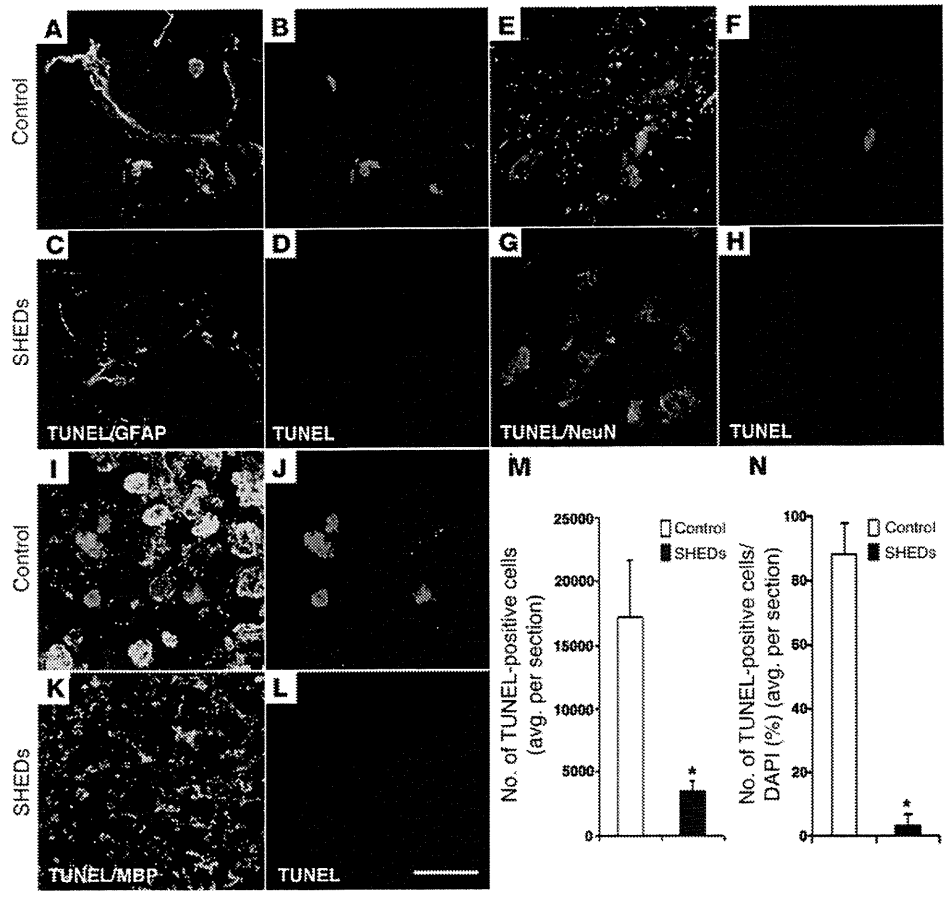


**Figure 8**
SHEDs suppress the apoptosis of neural cell lineages and secondary injury after SCI. Representative images (**A**–**L**) and quantifications (**M** and **N**) of apoptotic cell death 24 hours after SCI. Transverse sections 1 mm caudal to the epicenter of PBS-injected (**A**, **B**, **E**, **F**, **I**, and **J**) and SHED-transplanted SCs (**C**, **D**, **G**, **H**, **K**, and **L**) were stained with TUNEL and then subjected to immunohistochemical analysis with an anti-GFAP mAb (**A**–**D**), anti-NeuN mAb (**E**–**H**), or anti-MBP mAb (**I**–**L**). The engrafted SHEDs decreased the apoptotic cell death of all 3 neural cell lineages. (**M**) Quantification of the total TUNEL-positive cell number within 3 mm rostral and caudal to the epicenter shows the average of 3 experiments performed in parallel. (**N**) The percentage of TUNEL-positive relative to total DAPI-positive cell number in the same area as in **M**. Error bars represent SD. $^*P < 0.01$ compared with SCI models injected with PBS. Scale bar: 20 μm (**L**).

## Methods

*Isolation of SHEDs and DPSCs, and cell culture.* Human SHEDs and DPSCs were isolated as described previously (16, 17). Briefly, exfoliated deciduous teeth (from individuals 6–12 years old) and adult third molars (18–30 years old) extracted for clinical purposes were collected. After separation of the crown and root, the dental pulp was isolated and then digested in a solution of 3 mg/ml collagenase type I and 4 mg/ml dispase for 1 hour at 37°C. Single-cell suspensions ($1 \times 10^4$ to $2 \times 10^4$ cells/ml) were plated on culture dishes in DMEM supplemented with 10% fetal calf serum, then incubated at 37°C in 5% $CO_2$. Mesenchymal stem cells of three human bone marrow lines (hBMSCs, from individuals 20–22 years old) at passage 5 and three human skin-fibroblast lines (hFbs, 36–40-years old) at passage 5 were obtained from Lonza and the Health Science Research Resources Bank Japan, respectively.

*Real-time PCR and microarray analysis.* Total RNA was quantified by a spectrophotometer, and RNA integrity was checked on 1% agarose gels. RT reactions were carried out with Superscript III reverse transcriptase (Invitrogen) using 1 μg of total RNA in a 50 μl total reaction volume. Real-time PCR was performed using the THUNDERBIRD SYBR qPCR Mix (Toyobo) driven by the StepOnePlus Real-Time PCR System (Applied Biosystems). Primers were designed using DNADynamo (BlueTractorSoftware Ltd) and primer 3, as follows: *BDNF* forward (5′-GGGAAAAGGGAACAGGAAAA-3′), *BDNF* reverse (5′-AACAGACAGGATGGGCAGAA-3′), *GDNF* forward (5′-CGAACTCTTGCCCCTGACCT-3′), *GDNF* reverse (5′-ACAGCCACGACATCCCATAAC-3′), *CNTF* forward (5′-CCTTCTCTCTTCCTTGCTTTCTCTT-3′), *CNTF* reverse (5′-TGTCCCTGCTCCCACTCTCT-3′), *NT-3* forward (5′-TCAAAACGGGCAACTCTCCT-3′), *NT-3* reverse (5′-CTCGACAAGGCACACACACA-3′), *NGF* forward (5′-TTCCCTTGACACTGCCCTTC-3′), *NGF* reverse (5′-GATGATGACCGCTTGCTCCT-3′). Microarray experiments were carried out using a CodeLink Human Whole Genome Bioarray (Applied Microarrays Inc.) at Filgen Inc. The arrays were scanned using a GenePix4000B Array Scanner (Molecular Devices). The data were analyzed by using MicroArray Data Analysis Tool version 3.2 (Filgen Inc.) and deposited in the GEO database (accession GSE32403).

*Flow cytometry analysis.* For flow cytometry, $1 \times 10^6$ cells were incubated with FITC-conjugated primary mAbs against CD34, CD45, and CD11b and PE-conjugated against HLA-DR, CD105, CD73, and CD90 (BD Biosciences) at 4°C for 30 minutes and then washed twice with PBS containing 0.1% bovine serum albumin. The expression of intracellular markers was examined by indirect immunostaining. Cells were fixed with 4% (w/v) PFA for 5 minutes and permeabilized with 0.1% (v/v) Triton X-100 in PBS for 5 minutes. After blocking with 10% (v/v) goat serum for 30 minutes, the cells were incubated with primary Abs: anti-GFAP (mouse IgG, 1:500, Millipore), anti-βIII-tubulin (mouse IgG, 1:1,000, R&D Systems), anti-NeuN (mouse IgG, 1:100, Millipore), anti-CNPase (mouse IgG, 1:500, Millipore), anti-nestin (rabbit IgG, 1:500, Millipore), anti-DCX (guinea pig IgG, 1:500, Millipore), anti-APC (rabbit IgG, 1:300, Abcam), anti-MBP (rabbit IgG, 1:500, Abcam), anti-A2B5 mAb (mouse IgG, 1:500, Millipore). The secondary Abs were anti-mouse IgG, anti-rabbit IgG, and anti-guinea pig IgG-conjugated with Alexa Fluor 448 (Invitrogen), used at 1:1,000. Cell fluorescence was evaluated by flow cytometry using a FACSCalibur (BD Biosciences).

*Animal model and surgical procedure.* Adult female Sprague-Dawley rats were anesthetized with a mixture of xylazine (100–150 mg/kg) and ketamine (60–90 mg/kg). After laminectomy at the 9th–11th thoracic vertebral lev-

els, the dura was opened, and the SC was completely transected using a surgical blade (Feather surgical blade stainless steel no. 11). The severed ends of the SCs typically retracted about 1–2 mm. The rostral and caudal stumps were lifted to ensure complete transection. Then, $1 \times 10^6$ cells were drawn into a glass pipette with a tip diameter of 50–70 mm mounted onto a 10-μl Hamilton syringe attached to a micromanipulator. First, the cells were deposited into two injection sites at the rostral and the caudal stumps, 2 mm from the lesion and 0.5 mm lateral to the midline, at a depth of 1.5 mm. A 2.5-μl sample containing $2.5 \times 10^5$ cells in PBS was grafted into each site (injection rate, 0.8 μl/min). Next, $1 \times 10^5$ cells in fibrin glue were implanted into the 1- to 2-mm gap to fill the lesion site in the severed SC. After surgery, the rats were placed in temperature- and humidity-controlled incubation chambers until they awoke. They were then transferred to cages, and bladder evacuation was applied daily. Antibiotics (sodium ampicillin, 10 mg/kg body weight) were injected into the rats daily for a week. The rats were maintained under postoperative care for 8 weeks. All rats were given cyclosporine (Novartis) at 10 mg/kg/d on the day before surgery transplantation, then every day after surgery.

*Immunohistochemical analysis.* Cells were plated on PLL-coated 8-chamber slides and then incubated with the primary Abs listed above. For histological examination of the treated SCs, the animals were anesthetized and transcardially perfused with 4% PFA in 0.1 M PBS, 8 weeks after transplantation. The SCs were embedded in OCT compound (Sakura Finetek) and sectioned in the sagittal or transverse plane at 20 μm on a cryostat (Leica). The sections were incubated with primary Abs against human nuclei (mouse IgG, 1:100), NF-M (rabbit IgG, 1:300, Millipore), and 5-HT (rabbit IgG, 1:500, Sigma-Aldrich) in addition to the Abs listed above. Secondary Abs were anti-mouse IgG–Alexa Fluor 488, anti-rabbit IgG–Alexa 546, and anti-guinea pig IgG–Alexa 647. Myelin was stained by FluoroMyelin green dye (Invitrogen), according to the manufacturer's instructions. After counterstaining with DAPI (Sigma-Aldrich), cell images were captured with a confocal laser scanning microscope (A1Rsi, Nikon), while tissue images were taken with a universal fluorescence microscope (BZ9000, Keyence).

The differentiation activity of the engrafted SHEDs and the cells staining positive for MBP, APC, NF-M, or GFAP among the anti–human nuclei–positive transplanted cells were quantified. Cells were counted in at least 15 confocal images from 3 individuals in parallel experiments, with error bars representing SD.

*Anterograde neuronal tracing study.* For tracing of the CSTs, 0.5 μl of 5% biotinylated dextran amine (BDA: MW 10,000, Molecular Probes, Invitrogen; 5% in PBS) was injected into 4 sites in the hind limb area of the sensorimotor cortex at a 1.2-mm depth, following the rat brain atlas (54). Two weeks after the injections, sagittal cryosections (20 μm thick) of the SCs were prepared and processed by diaminobenzidine (DAB) staining with the ABC reaction protocol (VECTASTAIN Elite ABC, Vector Laboratories).

*BBB open field locomotor score.* Hind limb neurobehavioral testing was performed using the BBB locomotor rating scale (24). The 22-point (from 0 to 21) BBB scale was used to assess hind limb locomotor recovery, including joint movements, stepping ability, coordination, and trunk stability. A score of 21 indicates unimpaired locomotion as observed in uninjured rats. Two examiners who were blinded to the animal's treatments performed the tests. The duration of each session was 4 minutes per rat. The scores were analyzed by repeated-measures ANOVA with Tukey's multiple comparison tests at each time point.

*CM.* At 70%–80% confluence, the cell culture medium was changed to serum-free DMEM. After 48 hours incubation at 37°C in 5% $CO_2$, the CM was collected and centrifuged for 4–5 minutes at 4°C, 22,140 *g*. After the brief re-centrifugation, the supernatant was collected and used as CM.

*Neurite outgrowth assays.* Forty-eight-well tissue culture plates (Falcon, BD) were coated with 20 μg/ml PLL (Sigma-Aldrich) and then with 300 ng/ml extracellular CSPG mixture (Millipore) or 400 ng/ml MAG/Fc Chimera (MAG; Sigma-Aldrich) for 4 hours at 37°C. Rat CGNs were seeded onto PLL-, PLL/CSPG-, or PLL/MAG-coated 48-well tissue culture plates at $2.0 \times 10^4$ cells/well and cultured at 37°C in 5% $CO_2$ with SHED-CM, DPSC-CM, BMSC-CM, or fibroblast-CM. After 24 hours incubation, cells were fixed in 4% paraformaldehyde/PBS and stained with anti-neuron-specific βIII-tubulin (R&D Systems) to visualize neurites. Cell processes were defined as neurites when they were longer than the diameter of the cell body. Neurite length was evaluated by manually tracing neurite per cell using ImageJ software (version 1.29, http://rsbweb.nih.gov/ij/) and referenced to a known length. Each experiment was conducted in triplicate, and images were taken with 20 or more cells per field. For each experiment, at least 100 cells were randomly counted and measured.

*Analysis of apoptosis.* Apoptotic cell death was analyzed by TUNEL assay (In Situ Cell Death Detection kit, Roche). TUNEL-positive cells were counted on sections from sham-treated, PBS-injected, and SHED-transplanted animals. A researcher blinded to the experimental protocol determined the number of TUNEL-positive cells in the entire serial parasagittal section. The average number of TUNEL-positive cells per section was calculated from the values obtained by counting serial sagittal sections through the lesion site of each animal, with 3 animals examined per group.

*Statistics.* An unpaired 2-tailed Student's *t* test was used for single comparisons. For analysis of the real-time PCR results and open-field scores, we used repeated-measures ANOVA with Tukey's post hoc test (SPSS 19.0). A *P* value less than 0.05 was considered significant.

*Study approval.* The animal studies were carried out in accordance with the NIH Guidelines for the Care and Use of Laboratory Animals and approved by the Animal Research Committee of Nagoya University. Extracted teeth were collected at the Nagoya University School of Medicine, under approved guidelines set by Nagoya University (H-73, 2003). Ethical approval was obtained from the ethics committee of Nagoya University (permission number 8-2). All participants provided written informed consent.

## Acknowledgments

We are grateful to T. Yamashita (Osaka University) and M. Hibi (Nagoya University) for critical reading of the manuscript. We also thank T. Isa and T. Umeda (National Institute for Physiological Sciences); M. Koda and H. Takahashi (Chiba University); and M. Abematsu (Kagoshima University) for technical instruction. We are grateful to M. Fujio and R. Shohara for their comments and support of this study. We thank the Division of Experimental Animals and Medical Research Engineering, Nagoya University Graduate School of Medicine, for the housing of mice and for microscope maintenance. This work was supported by Grants-in-Aid for Scientific Research on Priority Areas from the Ministry of Education, Culture, Sports, Science and Technology of Japan; Grants-in-Aid for Practical Application of Regenerative Medicine from the Ministry of Health, Labour and Welfare of Japan; and COE for education and research of Micro-Nano Mechatronics Nagoya University Global COE Program.

Received for publication May 31, 2011, and accepted in revised form October 12, 2011.

Address correspondence to: Akihito Yamamoto, Department of Oral and Maxillofacial Surgery, Nagoya University Graduate School of Medicine, 65 Tsurumai-cho, Showa-ku, Nagoya 466-8550, Japan. Phone: 81.52.744.1978; Fax: 81.52.744.1978; E-mail: akihito@med.nagoya-u.ac.jp.

1. Norenberg MD, Smith J, Marcillo A. The pathology of human spinal cord injury: defining the problems. *J Neurotrauma.* 2004;21(4):429–440.
2. Schwab JM, et al. Experimental strategies to promote spinal cord regeneration – an integrative perspective. *Prog Neurobiol.* 2006;78(2):91–116.
3. Rowland JW, Hawryluk GW, Kwon B, Fehlings MG. Current status of acute spinal cord injury pathophysiology and emerging therapies: promise on the horizon. *Neurosurg Focus.* 2008;25(5):E2.
4. Yiu G, He Z. Glial inhibition of CNS axon regeneration. *Nat Rev Neurosci.* 2006;7(8):617–627.
5. Cummings BJ, et al. Human neural stem cells differentiate and promote locomotor recovery in spinal cord-injured mice. *Proc Natl Acad Sci U S A.* 2005; 102(39):14069–14074.
6. Keirstead H, et al. Human embryonic stem cell-derived oligodendrocyte progenitor cell transplants remyelinate and restore locomotion after spinal cord injury. *J Neurosci.* 2005;25(19):4694–4705.
7. Kumagai G, et al. Roles of ES cell-derived gliogenic neural stem/progenitor cells in functional recovery after spinal cord injury. *PLoS One.* 2009;4(11):e7706.
8. Erceg S, et al. Transplanted oligodendrocytes and motoneuron progenitors generated from human embryonic stem cells promote locomotor recovery after spinal cord transection. *Stem Cells.* 2010; 28(9):1541–1549.
9. Hofstetter CP, et al. Marrow stromal cells form guiding strands in the injured spinal cord and promote recovery. *Proc Natl Acad Sci U S A.* 2002; 99(4):2199–2204.
10. Cizkova D, Rosocha J, Vanicky I, Jergova S, Cizek M. Transplants of human mesenchymal stem cells improve functional recovery after spinal cord injury in the rat. *Cell Mol Neurobiol.* 2006; 26(7–8):1167–1180.
11. Sharp J, Keirstead HS. Therapeutic applications of oligodendrocyte precursors derived from human embryonic stem cells. *Curr Opin Biotechnol.* 2007; 18(5):434–440.
12. Deshpande DM, et al. Recovery from paralysis in adult rats using embryonic stem cells. *Ann Neurol.* 2006;60(1):32–44.
13. Kopen GC, Prockop DJ, Phinney DG. Marrow stromal cells migrate throughout forebrain and cerebellum, and they differentiate into astrocytes after injection into neonatal mouse brains. *Proc Natl Acad Sci U S A.* 1999;96(19):10711–10716.
14. Furuya T, et al. Treatment of rat spinal cord injury with a Rho-kinase inhibitor and bone marrow stromal cell transplantation. *Brain Res.* 2009; 1295:192–202.
15. Gronthos S, et al. Stem cell properties of human dental pulp stem cells. *J Dent Res.* 2002;81(8):531–535.
16. Gronthos S, Mankani M, Brahim J, Robey PG, Shi S. Postnatal human dental pulp stem cells (DPSCs) in vitro and in vivo. *Proc Natl Acad Sci U S A.* 2000;97(25):13625–13630.
17. Miura M, et al. SHED: stem cells from human exfoliated deciduous teeth. *Proc Natl Acad Sci U S A.* 2003;100(10):5807–5812.
18. Arthur A, Rychkov G, Shi S, Koblar SA, Gronthos S. Adult human dental pulp stem cells differentiate toward functionally active neurons under appropriate environmental cues. *Stem Cells.* 2008; 26(7):1787–1795.
19. Wang J, et al. Stem cells from human-exfoliated deciduous teeth can differentiate into dopaminergic neuron-like cells. *Stem Cells Dev.* 2010; 19(9):1375–1383.
20. Nosrat IV, Widenfalk J, Olson L, Nosrat CA. Dental pulp cells produce neurotrophic factors, interact with trigeminal neurons in vitro, and rescue motoneurons after spinal cord injury. *Dev Biol.* 2001; 238(1):120–132.
21. Nosrat IV, Smith CA, Mullally P, Olson L, Nosrat CA. Dental pulp cells provide neurotrophic support for dopaminergic neurons and differentiate into neurons in vitro; implications for tissue engineering and repair in the nervous system. *Eur J Neurosci.* 2004;19(9):2388–2398.
22. Huang AH-C, Snyder BR, Cheng P-H, Chan AWS. Putative dental pulp-derived stem/stromal cells promote proliferation and differentiation of endogenous neural cells in the hippocampus of mice. *Stem Cells.* 2008;26(10):2654–2663.
23. Arthur A, Shi S, Zannettino AC, Fujii N, Gronthos S, Koblar SA. Implanted adult human dental pulp stem cells induce endogenous axon guidance. *Stem Cells.* 2009;27(9):2229–2237.
24. Basso DM, Beattie MS, Bresnahan JC. A sensitive and reliable locomotor rating scale for open field testing in rats. *J Neurotrauma.* 1995;12(1):1–21.
25. Mirsky R, Winter J, Abney ER, Pruss RM, Gavrilovic J, Raff MC. Myelin-specific proteins and glycolipids in rat Schwann cells and oligodendrocytes in culture. *J Cell Biol.* 1980;84(3):483–494.
26. Bhat RV, et al. Expression of the APC tumor suppressor protein in oligodendroglia. *Glia.* 1996; 17(2):169–174.
27. In 't Anker PS, et al. Isolation of mesenchymal stem cells of fetal or maternal origin from human placenta. *Stem Cells.* 2004;22(7):1338–1345.
28. Romanov YA, Svintsitskaya VA, Smirnov VN. Searching for alternative sources of postnatal human mesenchymal stem cells: candidate MSC-like cells from umbilical cord. *Stem Cells.* 2003; 21(1):105–110.
29. Young HE, et al. Human reserve pluripotent mesenchymal stem cells are present in the connective tissues of skeletal muscle and dermis derived from fetal, adult, and geriatric donors. *Anat Rec.* 2001; 264(1):51–62.
30. Zuk PA, et al. Human adipose tissue is a source of multipotent stem cells. *Mol Biol Cell.* 2002; 13(12):4279–4295.
31. Nombela-Arrieta C, Ritz J, Silberstein LE. The elusive nature and function of mesenchymal stem cells. *Nat Rev Mol Cell Biol.* 2011;12(2):126–131.
32. Maekawa M, et al. Signaling from Rho to the actin cytoskeleton through protein kinases ROCK and LIM-kinase. *Science.* 1999;285(5429):895–898.
33. Winton MJ, Dubreuil CI, Lasko D, Leclerc N, McKerracher L. Characterization of new cell permeable C3-like proteins that inactivate Rho and stimulate neurite outgrowth on inhibitory substrates. *J Biol Chem.* 2002;277(36):32820–32829.
34. Yamashita T, Tohyama M. The p75 receptor acts as a displacement factor that releases Rho from Rho-GDI. *Nat Neurosci.* 2003;6(5):461–467.
35. Monnier PP, Sierra A, Schwab JM, Henke-Fahle S, Mueller BK. The Rho/ROCK pathway mediates neurite growth-inhibitory activity associated with the chondroitin sulfate proteoglycans of the CNS glial scar. *Mol Cell Neurosci.* 2003;22(3):319–330.
36. Dubreuil C, Winton M, McKerracher L. Rho activation patterns after spinal cord injury and the role of activated Rho in apoptosis in the central nervous system. *J Cell Biol.* 2003;162(2):233–243.
37. Hall A. Rho GTPases and the actin cytoskeleton. *Science.* 1998;279(5350):509–514.
38. Lehmann M, et al. Inactivation of Rho signaling pathway promotes CNS axon regeneration. *J Neurosci.* 1999;19(17):7537–7547.
39. Dergham P, Ellezam B, Essagian C, Avedissian H, Lubell WD, McKerracher L. Rho signaling pathway targeted to promote spinal cord repair. *J Neurosci.* 2002; 22(15):6570–6577.
40. Fournier AE, Takizawa BT, Strittmatter SM. Rho kinase inhibition enhances axonal regeneration in the injured CNS. *J Neurosci.* 2003;23(4):1416–1423.
41. Celik M, et al. Erythropoietin prevents motor neuron apoptosis and neurologic disability in experimental spinal cord ischemic injury. *Proc Natl Acad Sci U S A.* 2002;99(4):2258–2263.
42. Gorio A, et al. Recombinant human erythropoietin counteracts secondary injury and markedly enhances neurological recovery from experimental spinal cord trauma. *Proc Natl Acad Sci U S A.* 2002; 99(14):9450–9455.
43. Wang X, et al. P2X7 receptor inhibition improves recovery after spinal cord injury. *Nature Med.* 2004; 10(8):821–827.
44. Demjen D, et al. Neutralization of CD95 ligand promotes regeneration and functional recovery after spinal cord injury. *Nature Med.* 2004;10(4):389–395.
45. Stirling DP, et al. Minocycline treatment reduces delayed oligodendrocyte death, attenuates axonal dieback, and improves functional outcome after spinal cord injury. *J Neurosci.* 2004;24(9):2182–2190.
46. Teng YD, et al. Minocycline inhibits contusion-triggered mitochondrial cytochrome c release and mitigates functional deficits after spinal cord injury. *Proc Natl Acad Sci U S A.* 2004;101(9):3071–3076.
47. Bush TG, et al. Leukocyte infiltration, neuronal degeneration, and neurite outgrowth after ablation of scar-forming, reactive astrocytes in adult transgenic mice. *Neuron.* 1999;23(2):297–308.
48. Faulkner JR, Herrmann JE, Woo MJ, Tansey KE, Doan NB, Sofroniew MV. Reactive astrocytes protect tissue and preserve function after spinal cord injury. *J Neurosci.* 2004;24(9):2143–2155.
49. Okada S, et al. Conditional ablation of Stat3 or Socs3 discloses a dual role for reactive astrocytes after spinal cord injury. *Nature Med.* 2006; 12(7):829–834.
50. Herrmann JE, et al. STAT3 is a critical regulator of astrogliosis and scar formation after spinal cord injury. *J Neurosci.* 2008;28(28):7231–7243.
51. Rolls A, Shechter R, Schwartz M. The bright side of the glial scar in CNS repair. *Nat Rev Neurosci.* 2009;10(3):235–241.
52. Keirstead HS. Stem cells for the treatment of myelin loss. *Trends Neurosci.* 2005;28(12):677–683.
53. Thuret S, Moon LDF, Gage FH. Therapeutic interventions after spinal cord injury. *Nat Rev Neurosci.* 2006;7(8):628–643.
54. Paxinos G, Watson C. *The Rat Brain in Stereotaxic Coordinates.* 2nd ed. Orlando, Florida, USA: Academic Press; 1986.

TISSUE ENGINEERING: Part A
Volume 18, Numbers 13 and 14, 2012

DOI: 10.1089/ten.tea.2011.0325

# Conditioned Media from Mesenchymal Stem Cells Enhanced Bone Regeneration in Rat Calvarial Bone Defects

Masashi Osugi, D.D.S., Wataru Katagiri, D.D.S., Ph.D., Ryoko Yoshimi, D.D.S., Ph.D., Takeharu Inukai, D.D.S., Hideharu Hibi, D.D.S., Ph.D., and Minoru Ueda, D.D.S., Ph.D.

Tissue engineering has recently become available as a treatment procedure for bone augmentation. However, this procedure has several problems, such as high capital investment and expensive cell culture, complicated safety and quality management issues regarding cell handling, and patient problems with the invasive procedure of cell collection. Moreover, it was reported that stem cells secrete many growth factors and chemokines during their cultivation, which could affect cellular characteristics and behavior. This study investigated the effect of stem-cell-cultured conditioned media on bone regeneration. Cultured conditioned media from human bone marrow–derived mesenchymal stem cells (MSC-CM) enhanced the migration, proliferation, and expression of osteogenic marker genes, such as osteocalcin and *Runx2*, of rat MSCs (rMSCs) *in vitro*. MSC-CM includes cytokines such as insulin-like growth factor-1 and vascular endothelial growth factor. *In vivo*, a prepared bone defect of a rat calvarial model was implanted in five different rat groups using one of the following graft materials: human MSCs/agarose (MSCs), MSC-CM/agarose (MSC-CM), Dulbecco's modified Eagle's medium without serum [DMEM(−)]/agarose [DMEM(−)], PBS/agarose (PBS), and defect only (Defect). After 4 and 8 weeks, implant sections were evaluated using microcomputed tomography (micro-CT) and histological analysis. Micro-CT analysis indicated that the MSC-CM group had a greater area of newly regenerated bone compared with the other groups ($p<0.05$) and histological analysis at 8 weeks indicated that the newly regenerated bone bridge almost covered the defect. Interestingly, the effects of MSC-CM were stronger than those of the MSC group. *In vivo* imaging and immunohistochemical staining of transgenic rats expressing green fluorescent protein also showed that migration of rMSCs to the bone defect in the MSC-CM group was greater than in the other groups. These results demonstrated that MSC-CM can regenerate bone through mobilization of endogenous stem cells. The use of stem-cell-cultured conditioned media for bone regeneration is a unique concept that utilizes paracrine factors of stem cells without cell transplantation.

## Introduction

RECONSTRUCTION AND REPLACEMENT of bone loss, atrophy, and injury, including fracture, often need a certain amount of bone or other graft substitutes.

Autogenous bone graft is believed to be an effective method of bone grafting and is still regarded as the "gold standard" for bone augmentation procedures because of the available bone volume, its osteogenic potential, and the fact that numerous studies of this type of graft have been carried out. Although this well-studied technique has a good prognosis,[1] it requires significant donor-site morbidity.[2] These days, allografts and xenografts are commercially available.[3–5] However, in addition to being difficult to shape into the desired form, these materials have a potential risk of infection and of inducing an immune response.[4,5] Further, even though biomaterials have the advantage of unlimited availability, these materials also bring a risk of infection and have poor osteoinductivity.

On the other hand, the use of growth factors that regulate cellular chemoattraction, proliferation, and differentiation has begun to be recognized as a new method for bone regeneration. Recent studies confirmed that several growth factors, such as bone morphogenetic proteins (BMPs), insulin-like growth factor (IGF)-1 and −2, transforming growth factor-β1, platelet-derived growth factor (PDGF), and fibroblast growth factor (FGF)-2, could improve cellular ability to undergo osteogenesis by stimulating cellular events.[6–8] In particular, BMPs were regarded as effective factors for the processes of bone healing and have been adopted as graft

Department of Oral and Maxillofacial Surgery, Nagoya University Graduate School of Medicine, Aichi, Japan.

materials in clinical cases of craniofacial bone defects.[9,10] However, recent studies in orthopedics indicated unexpected effects of BMPs on clinical bone regeneration. Further, these growth factors are expensive and may exaggerate inflammatory responses.[11,12] In addition, application of a single growth factor imposes a limitation on the ability to regenerate bone. It has therefore been considered that a combination of a number of different factors will be better for optimizing bone regeneration, and several studies have investigated mixtures of two or more types of factors for bone regeneration.[13,14]

Langer and Vacanti first established the concept of tissue engineering[15] and regenerative medicine as a tool for a new clinical platform aimed at treatment of a whole spectrum of interactive diseases.[16,17] This concept involves the regeneration of tissues using stem cells, scaffolds, and growth factors, on the basis that stem cells play a leading role in tissue regeneration.

Mesenchymal stem cells (MSCs) were first reported as fibroblast-like cells elaborated from bone marrow that attached to tissue culture surfaces.[18] MSCs can be easily obtained from bone marrow or other sites and their pluripotent nature allows them to replicate without differentiating, and confers on them the ability to differentiate into lineages of mesenchymal tissue, including bone, cartilage, fat, and muscle.[19] Bone marrow MSCs have great potential for bone regeneration and clinical applications of MSCs are under way. We have previously used a mixture of human MSCs (hMSCs) from bone marrow and platelet-rich plasma (PRP) (hMSCs/PRP) for craniofacial reconstruction and dental implants, which are bone graft materials with predictable grafting success.[20] Bone regeneration using hMSCs/PRP has achieved a measure of success in clinical cases.[21] However, this procedure suffers from some problems, such as high capital investment, expensive cell culture, complicated safety and quality management issues regarding cell handling, and invasiveness of the procedure that is required for the collection of bone marrow MSCs from the patients. Moreover, recent studies of MSCs transplantation in spinal cord injury revealed that the implanted MSCs did not survive for a long time.[22] Additionally, it is well established that MSCs secrete a variety of growth factors and cytokines.[23] These findings suggest that the paracrine effects of growth factors and cytokines secreted from the implanted MSCs may promote tissue repair and regeneration and therefore transdifferentiation of the implanted MSCs remains controversial. For example, IGF-1, PDGF, and stromal-cell-derived factor (SDF)-1 are known to accelerate the migration of hMSCs in *in vitro* studies.[14,24] The paracrine effects of MSCs have been demonstrated in rodent models of ischemic limb[25] and wound healing.[23]

The paracrine factors secreted by MSCs can accumulate in the conditioned media during cell culture. The conditioned media of MSCs culture (MSC-CM) have been reported to serve multiple positive functions in tissue regeneration.[23,25] MSC-CM may induce not only stem cell homing or mobilization into the injured tissues, but also transdifferentiation into several lineages of mesenchymal tissue. If these characteristics of endogenous stem cells can be exploited for bone regenerative medicine, then MSC-CM may provide a substitute for *ex vivo* culture and implantation of MSCs. A lack of requirement for MSCs will help to reduce several of the existing problems with MSCs culture and implantation.

The purpose of this study was to evaluate the effect of stem-cell-cultured conditioned media on bone regeneration *in vitro* and *in vivo*, and to establish a novel bone regenerative medicine that does not require stem cell implantation.

## Materials and Methods

The overall experimental design is summarized in Figure 1.

### *Cell preparation*

All animal experiments undertaken in this study were performed in strict accordance with the protocols approved by the Institutional Animal Care Committee.

hMSCs were purchased from Lonza, Inc. (Walkersville, MD) and cultured in MSC basal medium (Lonza, Inc.) containing MSCGM SingleQuots (Lonza, Inc.) at 37°C in 5% $CO_2$/95% air. After primary culture, the cells were subcultured at a density of $\sim 1\times10^4$ cells/cm$^2$. hMSCs at the third to the ninth passages were used for experiments. Subconfluent hMSCs were trypsinized and used for cell implantation.

Rat MSCs (rMSCs) were isolated from 7-week-old Wistar/ST rats (Japan SLC Shizuoka, Japan) as previously reported.[26] Briefly, donor rats were sacrificed and the femora were dissected out. Using sterile conditions, the edge of each bone was cut, Dulbecco's modified Eagle's medium (DMEM; Gibco, Rockville, MD) was injected into the bone marrow using a 25-gauge syringe, the bone marrow cells were flushed out to the opposite side, and this maneuver was repeated several times. The marrow was then seeded into each tissue culture flask in DMEM containing antibiotic-antimycotic (100 units/mL penicillin G, 100 μg/mL streptomycin, and 0.25 μg/mL amphotericin B; Gibco) and the medium was supplemented with 10% fetal bovine serum (FBS). Three days after seeding, floating cells were removed and the medium was replaced with fresh medium. The adherent, spindle-shaped cells were passaged when the cells were approaching confluence. Adherent cells were collected using trypsin/EDTA, resuspended in fresh medium, and transferred to new flasks at a density of $1\times10^4$ cells/cm$^2$. Pluripotency of obtained cells for differentiation into classical mesenchymal lineage cells, including osteoblasts, adipocytes, or chondrocytes, was verified by using previously reported methods. These cells were used as rMSCs in this study (data not shown).[27] The results indicated that these cells had stem cell characteristics. The rMSCs obtained from cultures at the second to fourth passages were used for experiments.

### *Preparation of conditioned media*

hMSCs that were 70%–80% confluent were re-fed with serum-free DMEM containing antibiotic-antimycotic. The cell-cultured conditioned media were collected after a 48-h incubation. The collected, cultured conditioned media were defined as hMSCs-cultured conditioned media (MSC-CM) and were stored at 4°C or −80°C before being used for the following experiments.

### *Migration and proliferation of rMSCs*

Transwell dishes with 8-μm-pore filters (BD BioCoat Control Inserts; Becton Dickinson and Co., Franklin Lakes, NJ) were used for migration analysis. The second to fourth passages of rMSCs ($5\times10^5$ cells/cm$^2$) were seeded into the

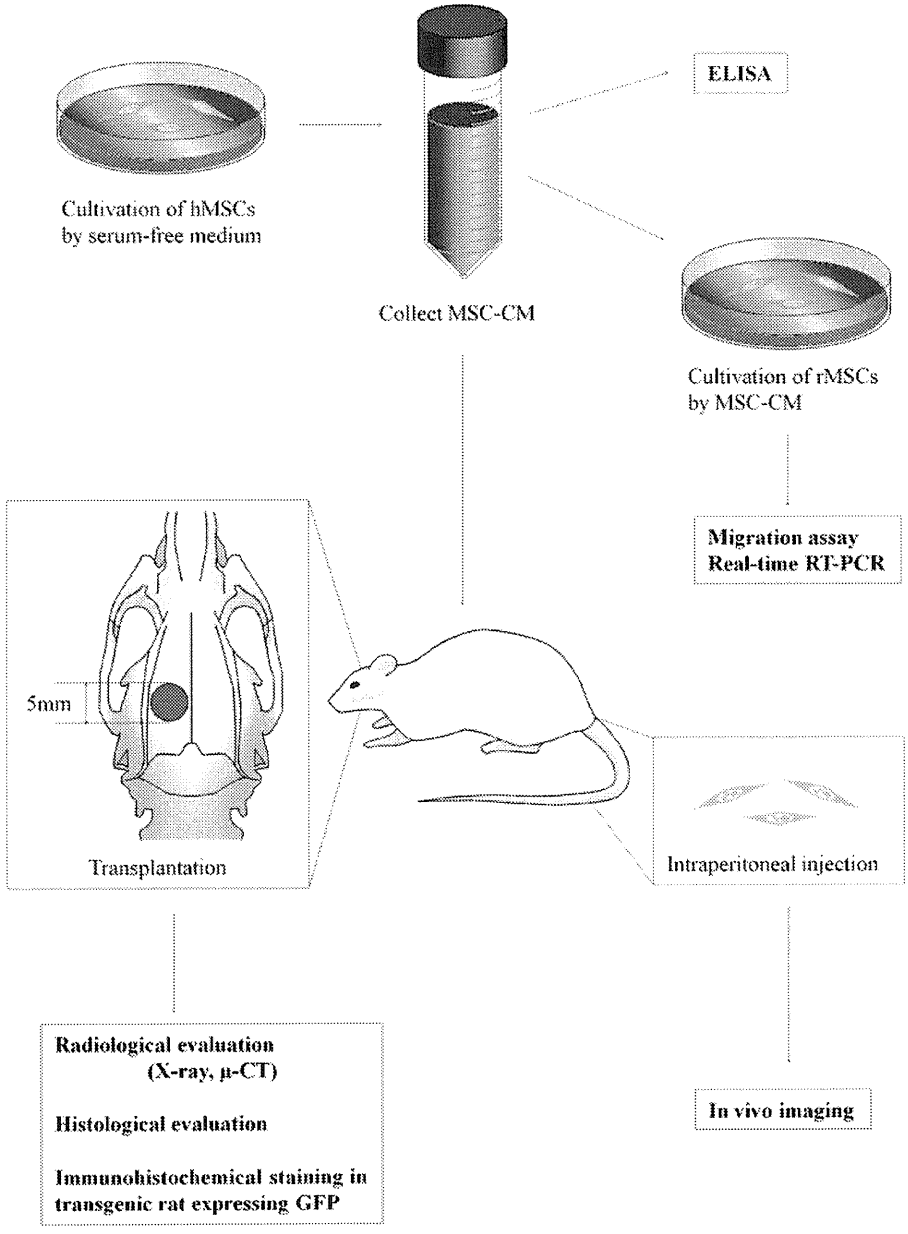


**FIG. 1.** Outline of the experimental protocol. MSC-CM was collected after cultivation of hMSCs for 48 h in serum-free medium. A rat calvarial bone defect of 5 mm in diameter was produced in each parietal bone. The effect of MSC-CM on cell migration, proliferation, and gene expression *in vitro*, and of implanted MSC-CM on bone regeneration *in vivo* were then analyzed as shown. hMSCs, human mesenchymal stem cells; CM, conditioned media; rMSCs, rat MSCs; RT-PCR, reverse transcriptase-polymerase chain reaction.

upper chamber, and MSC-CM was added to the lower chamber. To suppress cell proliferation without inhibiting cell survival, 0.25% FBS DMEM was placed into the upper chamber. Cell migration was observed in the presence of 30% FBS or serum-free DMEM, which served as positive and negative controls, respectively. After a 48-h incubation at 37°C in 5% $CO_2$/95% air, the upper side of the filters was carefully rinsed with phosphate-buffered saline (PBS) and remaining cells on the upper surface of the filters were mechanically removed with a cotton wool swab. Transwell filters were stained with hematoxylin, and then cut with a scalpel and mounted onto glass slides, with the lower surface facing upward. The total number of cells that had migrated was counted using a light microscope (CK40; Olympus, Tokyo, Japan) at ×200 magnification.

The proliferation rate of 70%–80% confluent rMSCs was assessed by bromodeoxyuridine (BrdU) incorporation for 24 h using a Zymed BrdU staining kit (Invitrogen, Carlsbad, CA) according to the manufacturer's instructions. The number of BrdU-positive cells was counted using a light microscope.

### *Enzyme-linked immunosorbent assay analyses*

The levels of IGF-1, vascular endothelial growth factor (VEGF), FGF-2, PDGF-BB, BMP-2, and SDF-1 in MSC-CM were investigated using enzyme-linked immunosorbent assay (ELISA). The concentration of these factors was measured using a Human Quantikine ELISA kit (R&D Systems, Minneapolis, MN) according to the manufacturer's

instructions. Briefly, 200 μL of MSC-CM, DMEM-0%FBS, or DMEM-30%FBS was added to 96-well microplates that were coated with a monoclonal antibody to the factor of interest and incubated for 2 h. After washing with PBS, a horseradish peroxidase-conjugated cytokine or growth-factor-specific antibody was added to each well, incubated for 2 h, and washed. Substrate solution was added and incubated for 30 min, and the reaction was terminated by addition of the stop solution. Cytokine/growth factor levels were determined by measurement of the optical density at 450 nm using a microplate spectrophotometer (Benchmark Plus; Bio-Rad, Hercules, CA).

### *Real-time reverse transcriptase–polymerase chain reaction analysis*

rMSCs were cultured with MSC-CM or DMEM-10%FBS (expansion medium [EM]) for 48 h, and total RNA was extracted using an RNeasy Mini kit (Qiagen GmbH, Hilden, Germany) according to the manufacturer's protocol. Real-time reverse transcriptase–polymerase chain reaction (RT-PCR) analysis was performed as previously described.[28,29] The sequence of the specific primers and probes used for the real-time RT-PCR analysis of Collagen type I alpha 2 (Col I), osteocalcin (OCN), *Runx2*, and *GAPDH* is listed in Table 1. RT-PCRs and the resulting relative increase in reporter fluorescent dye emission were monitored in real time using a 7000 Sequence Detector (Perkin-Elmer, Forster City, CA). Signals were analyzed using sequence detector software Ver. 1.1 (Perkin-Elmer). The PCR conditions were as follows: 1 cycle at 50°C for 2 min, 1 cycle at 60°C for 30 min, 1 cycle at 95°C for 5 min, 50 cycles at 95°C for 20 s (denaturation), and then 60°C for 1 min (annealing and extension).

The relative amount of each mRNA in one sample was obtained by calculation of the respective standard curves. The standard curves for each mRNA were drawn using different concentrations (2000, 400, 80, 16, and 3.2 ng) of the total RNA of rMSCs. The relative expression levels were normalized to *GAPDH* expression.

Table 1. Primer and Probe Sequences Used in the Real-Time Polymerase Chain Reaction

| *Gene* | *Sequence* | *Accession no.* |
|---|---|---|
| *Col I* | | |
| F | GACAGTCATTGAATACAAAAC | NM_053356 |
| R | ACGGAATTCTTGGTTAGTA | |
| Probe | TAAGCCATCTCGCCTGCCAT | |
| *OCN* | | |
| F | GACTCTGAGTCTGACAAA | NM_013414 |
| R | AGTCCATTGTTGAGGTAG | |
| Probe | CGGAGTCTATTCACCACCTTACTGC | |
| *Runx2* | | |
| F | CCTCTTATCTGAGCCAGA | NM_053470 |
| R | GCAGTGTCATCATCTGAA | |
| Probe | CATCCATCCATTCCACCACGC | |
| *GAPDH* | | |
| F | GTTCCAGTATGACTCTACC | NM_017008 |
| R | TCACCCCATTTGATGTTA | |
| Probe | TTCAACGGCACAGTCAAGGC | |

*Col I*, collagen type I alpha 2; *OCN*, osteocalcin.

### *Rat calvarial bone defect model*

Ten-week-old male Wistar/ST rats ($n=40$) were anesthetized by intraperitoneal injection of pentobarbital (Somnopentyl®; Kyoritsu Seiyaku, Tokyo, Japan) (20 mg/kg body weight). After shaving the skin, an L-shaped incision was made in the skull, and the periosteum was opened to expose the surface of the calvarial bones. Two circular bone defects (full-thickness, 5 mm in diameter) were made in calvarial bone using a trephine bur and were irrigated with saline to remove the bone debris. The experimental materials were then implanted into the defects. Agarose powder (Nusieve®; Cambrex Bioscience, Rockland, ME) (0.27 g) was suspended in 6 mL of PBS, serum-free DMEM, or MSC-CM, respectively. The suspension was heated at 37°C to dissolve the agarose, and cooled to room temperature. hMSCs ($1\times10^5$/defect) were mixed with PBS/agarose gel.

We defined the following groups based on the implanted materials: (1) MSC-CM: MSC-CM/agarose gel; (2) DMEM(−): serum-free DMEM/agarose gel; (3) PBS: PBS/agarose gel; (4) Defect: unfilled defect; (5) MSCs: hMSCs/agarose gel.

The rats were sacrificed at 4 or 8 weeks after transplantation ($n=4$ per group).

### *Radiographic and histological analyses*

Surgical sites were dissected, fixed in 10% formalin, and subjected to microcomputed tomography (micro-CT) analysis using a laboratory X-ray CT device (LATheta; Aloka Co., Tokyo, Japan). Images were compiled and analyzed to render 3D images using OsiriX® imaging software (Ver.3.9; www.osirix-viewer.com/). We then compared the area ($mm^2$) of newly regenerated bone.

After radiological assessment, explants were decalcified with K-CX solution (Falma Co., Tokyo, Japan) and were then dehydrated using graded ethanol, cleared with xylene, and embedded in paraffin. The specimens were cut in a sagittal direction to make 3-μm-thick histological sections and were stained with hematoxylin and eosin. Histological analysis was performed using a light microscope.

### In vivo *imaging analysis*

rMSCs were harvested and cultured as described previously and were labeled with the lipophilic tracer 1,1-dioctadecyl-3,3,3,3-tetramethylindotricarbocyanine iodide (DiR; Molecular Probes, Eugene, OR) for all imaging experiments.[30] This fluorophore is excited at 750 nm and has an emission peak at 782 nm. The cells were incubated with DiR ($3\times10^6$ cells in 10 mL PBS containing 3.5 μg/mL dye and 0.5% ethanol) for 30 min at 37°C. The cells were then washed twice with PBS and injected intravenously into the caudal vein of Wistar/ST rats with the bone defect described previously, which had been implanted with various implant materials just before the injection of rMSCs. The rats were anesthetized by intraperitoneal injection of Somnopentyl® prior to injection. Xenogen's IVIS® 200 Series Imaging System (Xenogen, Alameda, CA) was used to monitor DiR-labeled rMSC localization within live, as well as sacrificed, animals. Imaging was performed at 1, 24, and 48 h, and at 1 week after injection of DiR-labeled cells.

### *Immunohistochemical staining of CD44 in transgenic rats expressing green fluorescent protein*

Transgenic Sprague–Dawley rats [SD-Tg(CAG-EGFP)Cz-004Osb] carrying the enhanced green fluorescent protein (eGFP) transgene were obtained from Japan SLC, Inc. (Hamamatsu, Japan).[31] MSC-CM or PBS with agarose was implanted into calvarial bone defects of these transgenic rats and samples were collected after 4 weeks. Fresh-frozen sections of these samples were made according to the Kawamoto method by using a Multi-Purpose Cryosection Preparation Kit.[32] Cryofilm type 2C was applied to the cutting surface of the completely frozen block and the block was cut with a tungsten carbide knife at −25°C in a cryostat chamber (Leica CM3050S; Leica Microsystems, Wetzlar, Germany). The section was fixed with 100% ethanol for 10 min and then washed with PBS for 3 min. A mouse monoclonal anti-CD44 antibody (Cedarlane Laboratories Ltd., Hornby, Ontario, Canada) was used to detect MSCs.[33] An Alexa Fluor 633-conjugated goat anti-mouse IgG (Molecular Probes, Inc.) was used as the secondary antibody. After DAPI staining, the section was washed with PBS and mounted between a glass slide and the adhesive film. The section was enclosed by the mounting resin SCMM R2 on the glass slide and the resin was hardened with UV ray irradiation for 1 min by using the UV Quick Cryosection Mounter (ATTO Bio-Instrument, Tokyo, Japan). After fixation, the specimen was observed by fluorescence microscopy (BZ8000; Keyence Co., Osaka, Japan).

### *Statistical analysis*

All experiments were conducted in triplicate and repeated at least twice. Group means and standard deviations were calculated for each measured parameter. Statistical differences between two groups were evaluated using the Tukey-HSD test. Differences were considered statistically significant when the $p$-value was $<0.05$.

## Results

### *Effect of MSC-CM on rMSC*

The effect of MSC-CM on rMSC migration was determined using a transwell assay. The percentage of rMSCs that spontaneously migrated in the presence of the negative control, DMEM(−), was low (2.70%±0.9%), but migration increased in the presence of 30% FBS (47.4%±7.8%). MSC-CM significantly increased the migration rate of rMSCs compared with DMEM(−) (18.3%±4.1%). Thus, MSC-CM increased rMSC migration more than sevenfold compared with that in DMEM(−) (Fig. 2A).

The effect of MSC-CM on the proliferation of rMSCs was evaluated using a BrdU assay. The percentage of BrdU that was incorporated by rMSCs cultured in DMEM(−), 30% FBS, or MSC-CM was 19.94±6.29, 44.05±12.46, and 30.01±5.43 (%), respectively (Fig. 2B). These differences were statistically significant ($p<0.05$), indicating that MSC-CM also enhanced rMSC proliferation.

### *Growth factors present in MSC-CM*

The concentration of the growth factors IGF-1, VEGF, FGF-2, PDGF-BB, BMP-2, and SDF-1, released by hMSCs into MSC-CM, was quantified using ELISA analysis. Growth factors were not detected in DMEM-0% and DMEM-30%. However, MSC-CM contained IGF-1 and VEGF, at a concentration of 1386±465 and 468.5±109 pg/mL, respectively. The other factors assayed were not detected in MSC-CM (Table 2).

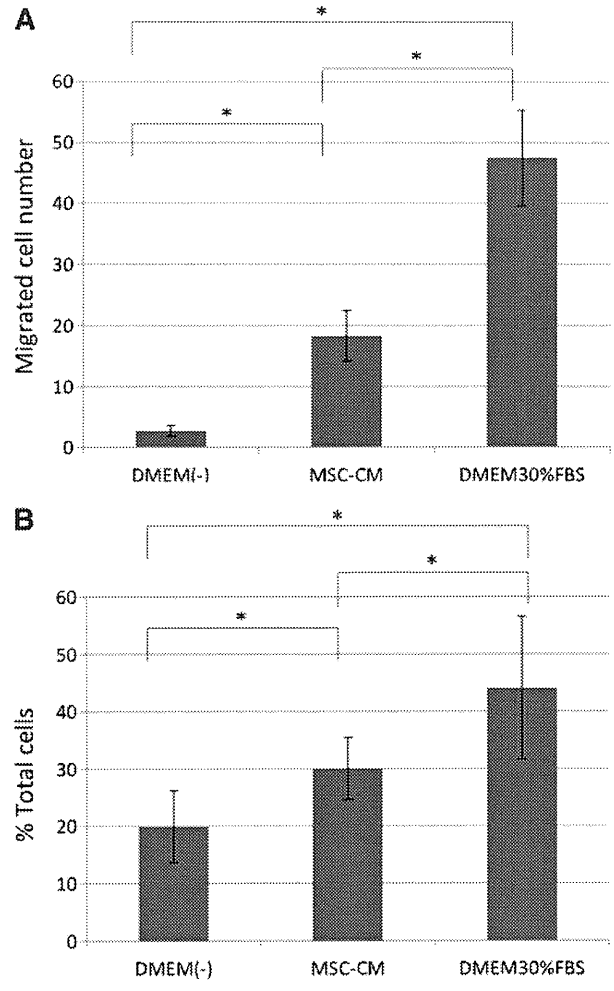


**FIG. 2.** Effect of MSC-CM on the migration and proliferation of rMSCs. **(A)** Transwell migration assay. The migration of rMSCs cultured in MSC-CM was enhanced compared with that of rMSCs cultured in DMEM(−). **(B)** BrdU cell proliferation assay. Proliferation of rMSCs was determined as the percentage of cells that incorporated BrdU. The proliferation of rMSCs was also enhanced when cultured with MSC-CM compared with culture in DMEM(−). Cells cultured in DMEM-30%FBS were used as a positive control for both **(A)** and **(B)**. Asterisks indicate a significant difference between the indicated groups (*$p<0.05$). FBS, fetal bovine serum; BrdU, bromodeoxyuridine; rMSCs, rat MSCs; DMEM, Dulbecco's modified Eagle's medium.

### *MSC-CM enhances osteogenic marker gene expression*

The effect of MSC-CM, or control DMEM-10%FBS (EM), on the relative mRNA expression of the osteogenic markers

TABLE 2. THE LEVELS OF CYTOKINES PRESENT IN MSC-CM

| *Factors* | *Concentration (pg/mL)* |
|---|---|
| IGF-1 | 1386±465 |
| VEGF | 465.8±109 |
| FGF-2 | ND |
| PDGF-BB | ND |
| BMP-2 | ND |
| SDF-1 | ND |

BMP-2, bone morphogenetic protein-2; IGF-1, insulin-like growth factor-1; VEGF, vascular endothelial growth factor; PDGF, platelet-derived growth factor; FGF, fibroblast growth factor; SDF-1, stromal-cell-derived factor-1; ND, not detected.

*Col I*, *OCN*, and *Runx2* by rMSCs was measured using real-time RT-PCR analysis. The levels of expression of the *OCN* and the *Runx2* genes were significantly upregulated in rMSCs cultured with MSC-CM compared with rMSCs cultured in EM (Fig. 3).

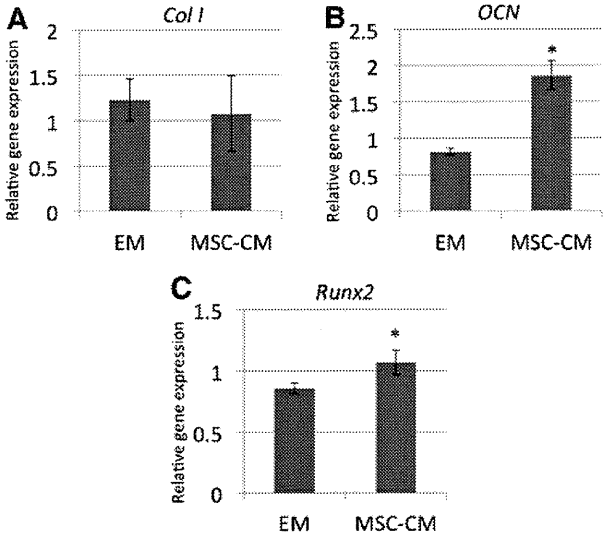


**FIG. 3.** Effect of MSC-CM on rMSC gene expression. The mRNA level of **(A)** *Col I*, **(B)** *OCN*, and **(C)** *Runx2* genes in rMSCs cultured in MSC-CM or DMEM-10%FBS (EM) was assayed using real-time reverse transcriptase–polymerase chain reaction. Cells were lysed for extraction of total RNA on day 7 of culture in MSC-CM or EM, and equal amounts of total RNA (50 ng) were analyzed. The mRNA expression levels of *Col I*, *OCN*, and *Runx2* were determined relative to the level of *GAPDH* mRNA in each sample and were quantified by calculation based on their standard curves as described in the Materials and Methods section. To quantitatively compare the levels of gene expression of the different samples, the expression coefficient for each mRNA on the ordinate was calculated by dividing the absolute level of expression of each mRNA (*Col I*, *OCN*, and *Runx2*) with the absolute level of expression of *GAPDH* mRNA in each sample. Each point represents the mean value calculated from five independent replicates, in which the difference was <10%. An asterisk indicates a significant difference between the EM and MSC-CM groups for the indicated gene (*$p<0.05$). *Col I*, collagen type I alpha 2; *OCN*, osteocalcin; EM, expansion medium.

### *MSC-CM enhances bone regeneration* in vivo

To determine whether MSC-CM could enhance bone regeneration, we implanted an MSC-CM/agarose composite gel, or various controls, into a rat calvarial bone defect (Fig. 4A). We then evaluated the area of newly regenerated bone as a percentage of the total graft area at 4 and 8 weeks after implantation, using micro-CT scanning (Fig. 4B).

After 2 weeks, areas of newly regenerated bone in the Defect, PBS, and DMEM(−) groups were <10% of the defect area, whereas the area in the MSC-CM group was over 20% (data not shown). After 4 weeks, bone defect areas were still seen in all groups. However, the area of newly regenerated bone in the MSC-CM group (49.5%±2.7%) was significantly increased compared with that in the Defect (23.4%±4.5%), PBS (24.9%±2.2%), and DMEM(−) (36.9%±1.8%) groups. This relative difference between the MSC-CM and the other groups was even stronger after 8 weeks, at which time the newly regenerated bone area of the MSC-CM group was very obvious and had increased to 64.4%±19.7% of the defect area. Thus, defect areas were almost filled by newly regenerated bone in the MSC-CM group 8 weeks after implantation. In contrast, the area of newly regenerated bone of the other three groups after 8 weeks was <50% [Defect: 28.6%±5.3%, PBS: 36.1%±2.9%, and DMEM(−): 44.9%±2.7%]. Thus, the MSC-CM group showed higher new bone regeneration in the peripheral area surrounding the defect compared with control groups after 2, 4, and 8 weeks. In contrast, bone regeneration of the hMSC-transplanted group (40.9%±5.0% at 4 weeks and 51.0%±3.7% at 8 weeks) was not as good as that of the MSC-CM group (Fig. 4C).

Histological analysis also showed well-regenerated bone in the MSC-CM group compared with the other groups. At 8 weeks, the bone bridge had almost covered the defect in the MSC-CM group and remnants of the agarose gel could not be observed. Calvarial bone regeneration was observed in the MSC group. In the PBS and DMEM(−) groups, some newly regenerated bone, as well as some remnants of the agarose gel, were seen, while in the Defect group most of the defect was filled with connective tissue. Inflammatory responses were not observed in any of the groups (Fig. 5).

### In vivo *imaging*

Migration of rMSCs to the implants *in vivo* was analyzed in rats of the different implantation groups in which DiR-labeled rMSCs were injected into the caudal vein. Although it is not possible to detect DiR-labeled cells at a great depth with the imaging system used, this system can detect DiR-labeled cells that accumulate on the calvarial bone. The fluorescent signal in all groups increased immediately after injection. In the control Defect group, the fluorescent signal of the labeled rMSCs was only detected in the tail and abdominal region at 1, 24, and 48 h, and at 1 week after injection. We confirmed that there were no signals at the defect area in the cranium at any time point. In the PBS group, fluorescent signals were observed in the tail and in the abdominal area at 24 and 48 h after injection, and very low signals were observed in the breast and cranial area after 1 week. In the MSC-CM group, a moderate increase in signal intensity was observed in the area of the tail and the abdominal region during the first 24 h after injection. At 48 h after injection, signal intensity in the MSC-CM-implanted area of the parietal bone started to increase. The maximum

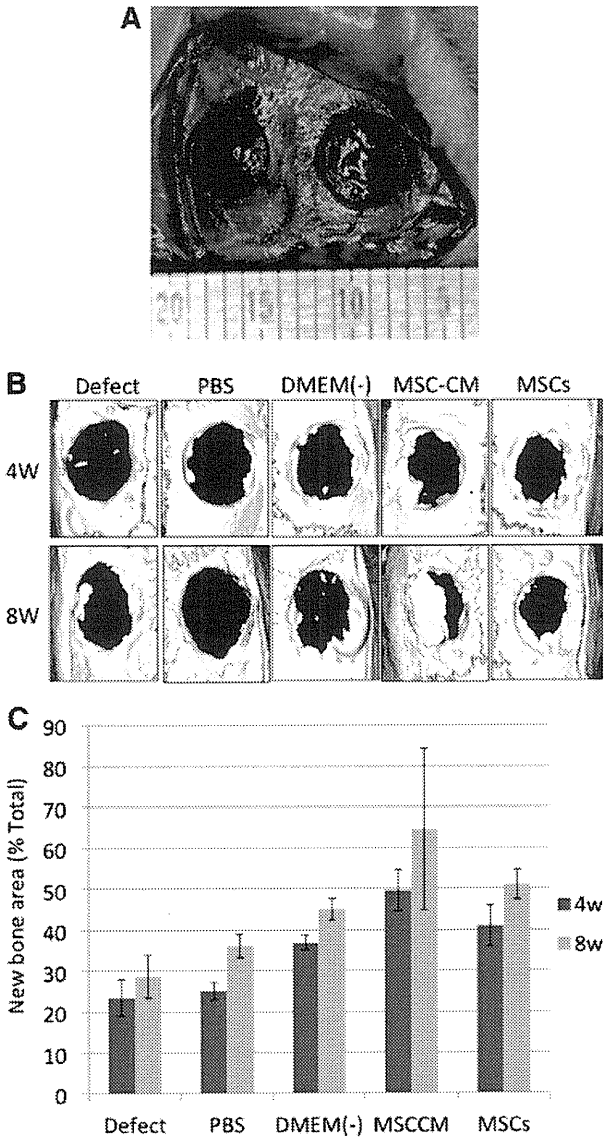


FIG. 4. Micro-CT analysis of bone regeneration following implantation of MSC-CM or controls into a bone defect. **(A)** Rat calvarial bone defects before implantation of the materials. A bone defect of 5 mm in diameter was prepared in each parietal bone. **(B)** Micro-CT images of the calvaria 4 and 8 weeks after implantation of the indicated materials. In the PBS, DMEM(−), MSC-CM, and MSCs groups, the materials were implanted as a mixture with an agarose gel, while in the Defect group, the defect was left unfilled. **(C)** The area of newly regenerated bone in each defect 4 and 8 weeks after implantation of the materials. The area of the newly regenerated bone ($mm^2$) was calculated for each of the experimental groups. The regenerated area is expressed as a percentage of the entire defect area. There were statistical differences between the area of the MSC-CM and that of the other groups both at 4 and 8 weeks except between the MSC-CM and MSCs groups at 8 weeks ($p < 0.05$). Micro-CT, microcomputed tomography; PBS, phosphate-buffered saline.

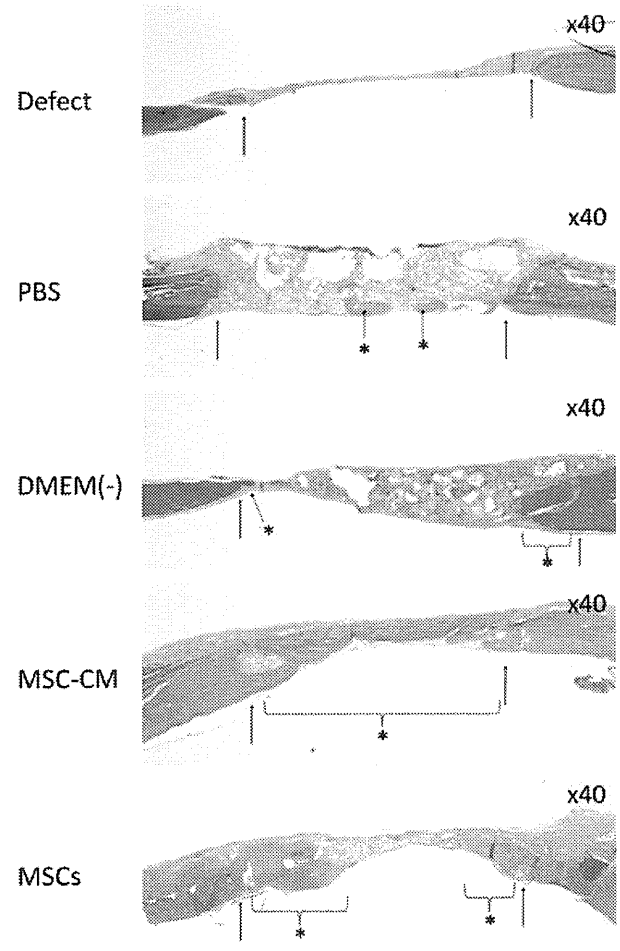


FIG. 5. Histological analysis of newly regenerated bone after implantation. Newly regenerated bone in the defect (Defect), PBS/agarose (PBS), DMEM(−)/agarose [DMEM(−)], MSC-CM/agarose (MSC-CM), and hMSCs/agarose (MSCs) groups was evaluated histologically. Hematoxylin and eosin staining of calvarial histological sections was performed 8 weeks after implantation. The arrows indicate the edges of the host bone and the dotted arrow and dotted line with asterisks indicate the newly regenerated bone. The bone bridge almost covered the defect in the MSC-CM group. In the MSCs group, partial regenerated bone was observed. Agarose gel remnants were not seen in these two groups. In the PBS and DMEM(−) groups, some newly regenerated bone and remnants of the agarose gel were seen, while in the Defect group most of the defect was filled with connective tissue. Inflammatory responses were not observed in any group. Color images available online at www.liebertonline.com/tea

fluorescent signal in the implanted area was observed 1 week after injection (Fig. 6).

### *Immunohistochemical staining of cells in regenerated bone in transgenic rats expressing GFP*

To confirm the mobilization of endogenous MSCs to calvarial defects by the transplanted MSC-CM, we immunohistochemically stained the cells in the regenerated

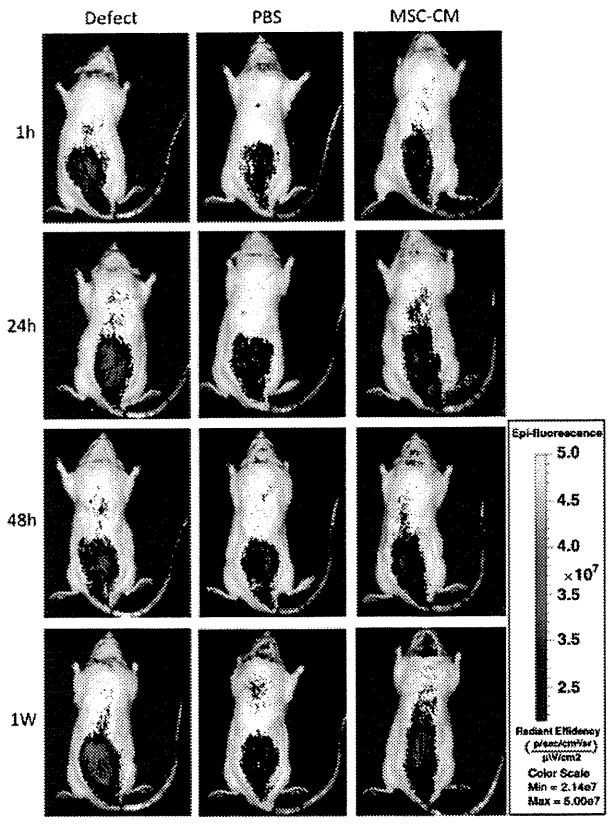


FIG. 6. *In vivo* imaging of injected rMSC migration to implants. *In vivo* imaging analysis shows that DiR-labeled rMSCs that were injected into the caudal vein just after implantation of the materials into the calvarial bone defects started to migrate immediately after injection. At 1 h, 24 h, 48 h, and 1 week after injection, the signal of the fluorescent-labeled rMSCs was only detected in the tail and abdominal region in the control Defect group. We confirmed that there was no signal at the defect area in the cranium at each time point. In the PBS group, fluorescent signals were observed in the tail and the abdominal area at 24 and 48 h after injection, and very low signals were observed in the breast and the cranial area after 1 week. In the MSC-CM group, a moderate increase in signal intensity was observed in the area of the tail and in the abdominal region during the first 24 h after injection. Forty-eight hours after injection, the MSC-CM-implanted area of calvarial bone started to increase in signal intensity, and, 1 week after injection, the MSC-CM implanted area showed the highest fluorescent signal of the experimental groups. Color images available online at www.liebertonline.com/tea

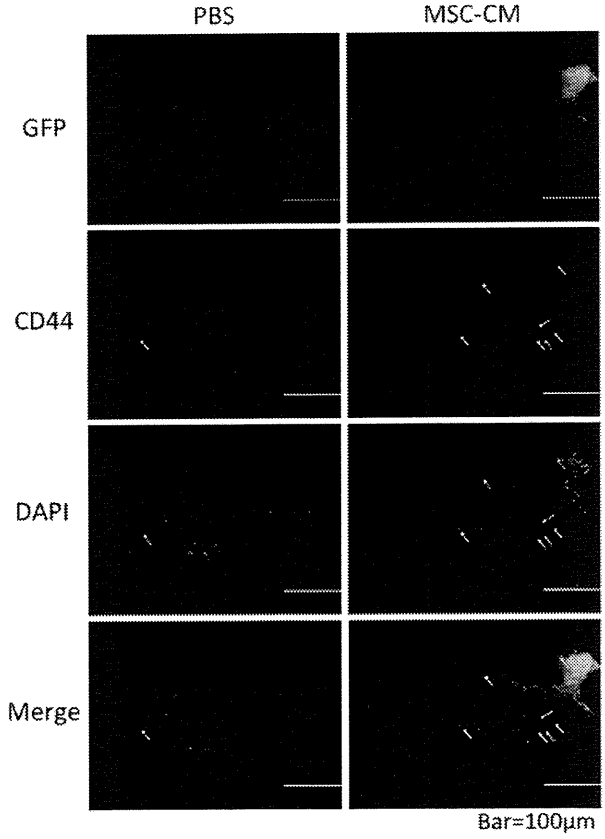


FIG. 7. Immunohistochemical staining of newly regenerated bone after implantation into transgenic rats expressing GFP. To detect endogenous MSCs in newly regenerated bone in calvarial bone defects, the calvarial bone defects of PBS/agarose (PBS) and MSC-CM/agarose (MSC-CM) groups of transgenic rats that expressed GFP were collected 4 weeks after implantation, and were immunohistochemically stained with anti-CD44 antibodies and Alexa Fluor 633-conjugated secondary antibodies. Nuclei were counterstained with DAPI. The arrows indicate CD44-positive cells (red) and nuclei (blue). In the MSC-CM group, a number of cells in the newly regenerated bone displayed both CD44 and GFP staining, whereas in the PBS group there were fewer CD44-positive cells. GFP, green fluorescent protein.

bone of transgenic rats expressing GFP with an anti-CD44 antibody and a fluorescent-labeled second antibody. Cell nuclei were labeled with DAPI (blue). A number of the cells in the newly regenerated bone in the MSC-CM group displayed both CD44 (red) and GFP (green) expression. In contrast, there were fewer CD44/GFP double-positive cells in the PBS group (Fig. 7).

## Discussion

The clinical application of MSCs suffers from a number of problems, including high cost, safety and cell handling issues, and invasive collection procedures. Although bone marrow MSC implantation has beneficial effects on specific diseases, the implanted MSCs do not survive for a long time but disappear 2 to several weeks after transplantation.[25] It has been proposed that paracrine mechanisms triggered by growth factors and cytokines secreted by the implanted MSCs may explain the benefit that is observed after MSC implantation.[23,25] Since the paracrine factors secreted by MSCs can accumulate in the conditioned media,[23] we therefore determined whether MSC-CM contains factors that regulate cell mobilization and osteogenic differentiation. The possibility of enhancing new bone regeneration by implantation of MSC-CM rather than of stem cells is a novel concept in tissue engineering and regenerative medicine. This novel bone regenerative medicine may also reduce the cost and shorten the duration of therapy.